

A novel method for tuning the biodegradation rate of poly-3-hydroxybutyrate by adding acidified biochar or oxidized biochar

Dagmar ŠAŠINKOVÁ^a, Markéta JULINOVÁ^{a*}, Alena KALEDOVÁ^b, Martina KASZONYIOVÁ^b, Antonín MINAŘÍK^c, Markéta KADLEČKOVÁ^{c,d}, Nurjahan MAHMUDOVA^a, Jana ŠERÁ^a and Marek KOUTNÝ^a

^a*Department of Environmental Protection Engineering, Faculty of Technology, Tomas Bata University in Zlín, Nad Ovčírnou 3685, 760 01, Zlín, Czech Republic, phone +420 576 031 220, email: julinova@utb.cz*

^b*Department of Polymer Engineering, Faculty of Technology, Tomas Bata University in Zlin, Vavrečkova 5669, 760 01 Zlín, Czech Republic*

^c*Department of Physics and Material Engineering, Faculty of Technology, Tomas Bata University in Zlin, Vavrečkova 5669, 760 01 Zlin, Czech Republic*

^d*Centre of Polymer Systems, Tomas Bata University in Zlín, Třída Tomáše Bati 5678, 76001 Zlín, Czech Republic*

***Corresponding author:**

M. Julinová: Department of Environmental Protection Engineering, Faculty of Technology, Tomas Bata University in Zlín, Nad Ovčírnou 3685, 760 01, Zlín, Czech Republic; email julinova@utb.cz, tel. +420 576 031 220

Abstract

This study revealed that the acidification and oxidation of biochar retarded the biodegradation of poly-3-hydroxybutyrate (PHB) films to a different extent. This finding is important as it both contributes to research efforts on PHB-based products and comprehending what happens to PHB and PHA (polyhydroxy acid) following their release into a natural environment. Herein, film samples were fabricated from neat poly-3-hydroxybutyrate and PHB supplemented with various forms of biochar (1 wt%) by extrusion and thermocompression. The properties of the films were investigated by optical microscopy, scanning electron microscopy (SEM), atomic force microscopy, differential scanning calorimetry, thermogravimetric analysis and X-ray diffraction. The PHB films underwent a biodegradation test in earth, the biological agent employed for this being natural mixed microflora in the form of garden soil. The course and extent to which they biodegraded were gauged by respirometry to determine the amount of carbon dioxide produced through microbial degradation. SEM, fluorescence microscopy and next-generation sequencing were carried out to study the microbial community involved in the biodegradation of the films. Investigation was also made of the environmental impacts of samples, discerning how they broke down in river sediment, in addition to which a phytotoxicity screening test was conducted. Analysis revealed that the thermal properties of the filled films were comparable to those of the neat PHB specimen. Respirometric data indicated the extent of PHB biodegradation could be adjusted by adding biochar, discerned as 87% in mineralization for the neat PHB material and 37% to 64% for the filled samples after 7 months. The rate of such biodegradation depended on how the biochar had been chemically modified. The hydrophilicity of the polymer surface did not relate to the lag phase or aforementioned biodegradation rate in the soil. Sequence analysis

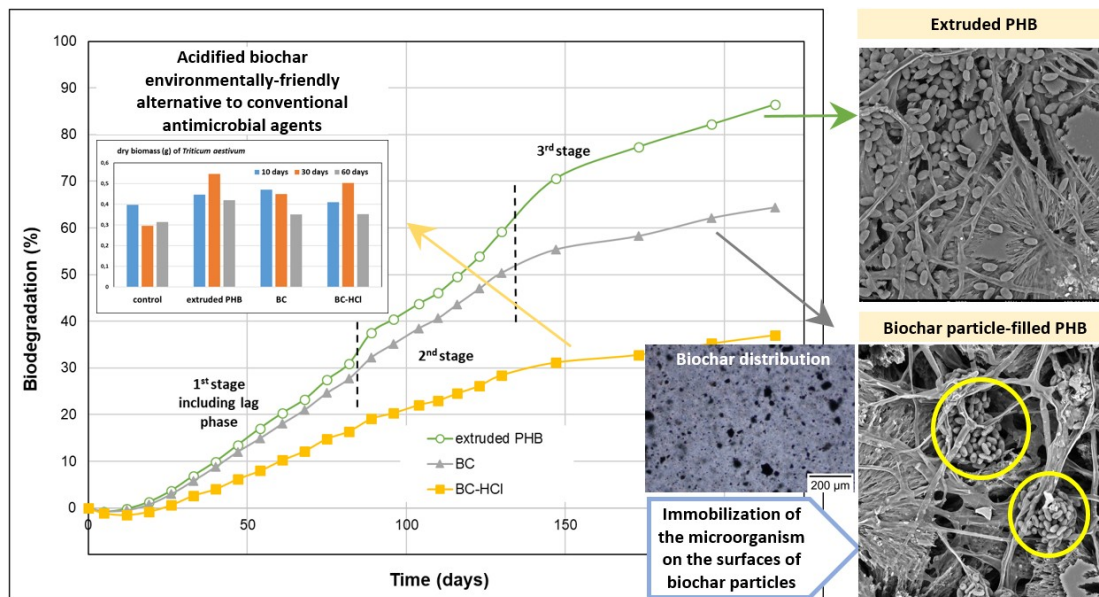
suggested that the biofilm communities that initially colonized the films were influenced by the type of biochar in their polymer matrices. Findings showed that the PHB materials supplemented with the modified biochar did not impact the cultivation of plants or the river environment. Notably, every film had degraded in river environment by over 50% in just a month.

Keywords: poly-3-hydroxybutyrate, biodegradation, acidified biochar, oxidized biochar, soil environment, river sediment, sustainable biomaterials

Highlights

- Acidified biochar and oxidized biochar act as agents for controlling the biodegradation of PHB in soil.
- The modified biochar represents an environmentally-friendly alternative to conventional antimicrobial agents.
- Soil microorganisms are immobilized on the surface of the biochar during the biodegradation process.
- The experimental PHB film, filled with modified biochar, makes no discernible impact on a river environment.
- No phytotoxic effect is exerted on plants as a consequence of biodegradation by the tested film.

Graphical abstract



1. Introduction

Poly-3-hydroxybutyrate is a highly crystalline thermoplastic biopolymer. An aliphatic and 100% isotactic stereoregular polyester insoluble in water, it exhibits high moisture resistance and excellent gas barrier properties, in addition to being optically active, piezoelectric and biodegradable. Such properties mark it out as a promising alternative to forms of petroleum-based plastic. The relatively high rate to which it biodegrades limits its potential for application, however. Great interest has been shown in recent years in attempting to control or regulate its rate of degradation, a matter which has presented a major challenge to those devising novel biodegradable polymer systems.

Several solutions to it are reported in the literature with regard to the biodegradability of polylactic acid (PLA), polycaprolactone (PCL), polyhydroxyalkanoate (PHA) and PHB, amongst others [1].

One option is to employ synthetic organic antimicrobial agents or fillers, e.g. halogenated compounds, quaternary ammonium salts, ethylenediaminetetraacetic acid, propionic acid, benzoic acid, sorbic acid and synthetic disinfectants [2].

The second way is to prepare polymer blends from a combination of PHA or PHB with natural antimicrobial agents or fillers, including biopolymers (chitosan and chitin) [2-4], antimicrobial compounds (vanillin, nisin, thymol, carvacrol, eugenol, isothiocyanate and antibiotics) [2,5-7], essential oils (derived from grapeseed, bergamot or ginger) [8] and enzymes (peroxidase, lysozyme) [2,5].

Another approach is to blend PHA with nanoparticles, most commonly those of inorganic antimicrobial agents, e.g. silver, copper, gold and platinum, or metal oxide nanoparticles like TiO_2 , ZnO and MgO [1,2,9,10]. A synergic effect between an organic or inorganic compound and nanoparticles can also be leveraged; quaternary ammonium-modified montmorillonite [2,11], Ag zeolite and an essential oil with MgO [8] are applicable in this regard.

A number of factors need to be taken into account when developing materials with a controlled lifetime, as even supplementing a tiny amount of an antimicrobial agent could change the technological and user-facing aspects of the final product. The choice of active compounds depends on the properties of the material and their mutual compatibility, especially resistance to temperature, solubility and differences in polarity. Organic compounds, for instance, such as chitosan or its derivatives, essential oils, organic acids and enzymes, prove highly sensitive to demanding processing conditions, including high temperatures and pressures during extrusion

[12,13]. The physicochemical properties and microbial diversity of the given environment are also important. Every factor mentioned above is decisive with regard to ensuring the maximum effectiveness of the active compounds. In the case of nanoparticles, it is necessary to carry out an assessment of the risks posed by them to aquatic and terrestrial systems. Discussion in this context centres on crisis factors, namely the quantity of them and their size, morphology, toxicity and migration rate. No legal regulations exist as that directly pertain to the ecological impact or safety of nanoparticles, as research has not yielded any clear conclusions on the matter.

The findings reported herein came about through broader research conducted on polymer composites supplemented with biochar, in connection with its porous structure, large surface area and high carbon content. Efforts initially focussed on preparing films of PHB and chemically modified biochar, with the aim of ensuring a good dispersion of the latter in the polymer matrix. This explains the various forms of biochar tested, as modified by acidification or an oxidizing agent. In the course of experiments on the fundamental properties and biodegradation of the PHB/biochar materials, a significant retardation in the biological degradation of some samples was observed, which proved of great interest as biochar generally supports biological processes. Further investigation ensued, leading to the data reported in this study. A notable aspect is that the chemically modified biochar remains stable during the extrusion process, hence it could represent an ecological alternative to a conventional antimicrobial agent; as for the latter, when incorporated in a polymer matrix, a residue exists after the plastic substance has decomposed, constituting an environmental impact [14-18].

Description is given herein of the preparation, characterization and biodegradation of PHB films filled with chemically modified biochar (1 wt%). Their properties were variously analysed,

as follows: optical and atomic force microscopy, attenuated total reflectance infrared spectroscopy, differential scanning calorimetry, X-ray diffraction analysis, water uptake and surface wettability. The influence of the chemically modified biochar on the course, rate and extent of biodegradation of the PHB films in soil was investigated by a respirometric test, in terms of the carbon dioxide produced. Further assessment covered changes in the diversity and quantity of microbiocenosis during biodegradation, through performing surface studies by fluorescence microscopy and sequencing analysis of the microbial communities present. Evaluation also encompassed the environmental impact of the biodegradable materials and how they affected the growth of *Triticum aestivum*.

2. Materials and methods

2.1 Materials and Chemicals

Poly-3-hydroxybutyrate (technical grade and additive free), biosynthesized from *Cupriavidus necator* with the medium of D-glucose (M_n 87 910 g.mol⁻¹, M_w 437 900 g.mol⁻¹, M_z 1 350 000 g.mol⁻¹; dispersity index of 4.98, as revealed by GPC [19]), was purchased from the Tianan Biologic Materials Co. Ltd. (China). The biochar was kindly supplied by M. Pohořelý (Institute of Chemical Process Fundamentals at CAS, Czech Republic). The remaining chemicals employed were of analytical grade without further purification, and produced by or sourced from Pliva Lachema Brno (Czech Republic).

2.2 Biochar modification

Prior to modification, the biochar (BC) was ground up in a ball mill (Retsch MM 301 Mixer Mill, Germany) to a particle size of less than 1 μm .

Acid treatment of biochar: In accordance with Mahmoud et al. [20], the process transpired as follows. An amount of biochar was washed with solutions of the given acid (1M HCl or 3M MA) three times, and with hot distilled water afterwards. The samples were then dried in an oven at 100°C overnight. The resulting products (HCl-TREATED and MA-TREATED) were stored in a closed box for later use.

Biochar-surface oxygenation with hydrogen peroxide: A procedure described by Xue et al. [21] and Huff & Lee [22] was adhered to, whereby the biochar was treated with H_2O_2 in water. 15 g of the biochar was added into 200 ml Erlenmeyer flasks, followed by 100 ml of 10% w/w H_2O_2 solution. This suspension underwent stirring for 2 hours at 300 rpm, upon which the sample was filtered through filter paper and washed three times with cold distilled water to remove any residual H_2O_2 . The samples were then dried in an electric drying oven at 80°C overnight. The resulting product (H_2O_2 -TREATED) was stored in a closed container for later use.

2.3 Processing the materials

PHB and PHB-biochar films containing 1 wt% of BC were prepared, commencing with extrusion on a twin-screw microcompounder (HAAKE Minilab, USA, Thermos Fisher) at a temperature of 185°C and 50 rpm, under a nitrogen atmosphere. The melt-processed films (ca 120x120x0.1 mm in dimension) were obtained by thermocompression on a hydraulic press at 185°C and 5 kg cm^{-2} , this stage lasting 3 minutes. The thicknesses of the films were measured

with a digital caliper (MAX-CAL, Fowler & NSK, Japan). At least 10 measurements were taken for each specimen, from which mean values were calculated for thickness (Table 1). A total of five different films were produced in this manner, denoted according to the process for biochar modification: PHB (control); PHB with non-treated (also referred to herein as “untreated”) biochar (BC); and PHB with chemically modified biochar (BC-HCl, BC-MA and BC-H₂O₂).

Table 1

2.4 Scanning electron microscopy (SEM)

The morphologies of the PHB and PHB-biochar films were gauged on a scanning electron microscope (a Phenom Pro X device equipped with the Pro Suite; Phenom-World BV, Eindhoven, Netherlands). Images were taken at the magnification of 3000x or 5000x. The unit was set to the acceleration voltage of 10 kV.

2.5 Film characterization with polarized optical microscopy (POM)

Polarized Light Microscopy was applied to discern the crystallization morphology and interference colour for every sample (PLM, Nikon Eclipse 50i; Nikon, Japan). The resulting scale bar was produced in ImageJ software, version 1.5 (W. Rasband, National Institutes of Health, United States).

2.6 Atomic force microscopy (AFM)

In agreement with another paper by the Julinova et al. [23], changes in surface topography and phase contrast were characterized on an Ntegra-Prima atomic force microscope (NT-MDT Spectrum Instruments, Moscow, Russia). Measurements were taken at a scan speed of 0.5 Hz, at the resolution of 512 x 512 pixels, and in tapping mode at room temperature in an air atmosphere. A silicone-nitride probe with a resonant frequency of 87 - 230 kHz and stiffness constant of 1.45 - 15.1 N m⁻¹ (NSG01, NT-MDT) was employed. The amount of the filler at surface was evaluated by analysing phase images in ImageJ 1.54f software (Wayne Rasband, National Institutes of Health, USA). The extent of surface roughness, denoted as Sa, was obtained via Gwyddion 2.63 software (Czech Metrology Institute); this represented the arithmetical mean as a maximum, constituting an absolute value for the difference in height at each point with reference to the mean for the entire surface of the sample [23].

2.7 Qualitative X-ray fluorescence analysis (XRF)

Qualitative X-ray fluorescence analysis (XRF) was conducted on an ElvaX SER-01 (Elvatech Ltd., Ukraine) unit fitted with a silver X-ray lamp. Measurement was carried out at the current of $I = 64 \mu\text{A}$ and anode voltage of 10 kV, while the exposure time for each sample lasted 100 seconds. The samples were placed in special polyethylene accessories equipped with polypropylene film.

2.8 Attenuated Total Reflectance Infrared Spectroscopy (FTIR)

FTIR spectra for the samples of biochar, extruded PHB and the PHB-biochar films were recorded on a FTIR Nicolet iS10 unit (Thermo Scientific, USA) equipped with an ATR Smart MIRacle™ adapter and a diamond crystal. The analysis comprised 64 scans at wave numbers ranging from 4000 to 500 cm⁻¹ and the spectral resolution of 4 cm⁻¹. The data gathered was evaluated in Omnic 8 software (Thermo Scientific, USA).

2.9 X-ray diffraction analysis (XRD)

An XRDynamic 500 (Anton Paar s.r.o, Austria) was employed for XRD, in which CuK_α radiation was Ni-filtered and scans (5° 2θ/min.), in reflection mode, occurred across the 2θ range of 5-50° at room temperature and in an air atmosphere.

2.10 Thermal Analysis

In preparation for differential scanning calorimetry (DSC) measurements, 5 mg of dried sample was weighted in standard aluminium crucibles. The given specimens were analysed on a Mettler Toledo DSC1 STAR calorimeter in a temperature scan from -30°C to 200°C at 10°C/min. The degree of crystallinity (X_c , %) of the PHB and PHB-biochar films was calculated according to Eq. 1, where ΔH_m represents the melting enthalpy of the sample (the tested films), ΔH_0 constitutes the melting enthalpy in J/g of 100% crystalline PHB (146 J/g) and w is the weight of sample. [24]

$$X_c = \left[\Delta H_m / (\Delta H_0 \times w) \right] \times 100 \quad (1)$$

Thermogravimetric analysis (TGA) was performed on STA 449 F1 Jupiter unit fitted with FTIR Bruker Alpha II accessories. Measurements were taken in a scan from 30°C to 600°C at a heating speed of 10°C/min., for samples which had been placed in corundum crucibles (cca 15 mg). Testing was conducted in air to simulate real environmental conditions.

2.11 Surface wettability - Water contact angle (WCA)

Surface wettability was determined by gauging water contact angles for samples, via the sessile drop method on a Contact Angle Meter DSA30 (Krüss). This involved dosing approximately 10 µl of distilled water by an automatic pipette onto the surfaces of the films, which were then photographed and evaluated by a three-point process (error ± 5%) in Krüss Advance software.

2.12 Water uptake test

Water uptake was assessed by a gravimetric method, whereby specimens of the PHB and PHB-biochar films (stored at laboratory temperature) of specific size (10 mm × 10 mm) were weighed out and placed in a humidity chamber (54% RH, 25°C). The difference in weight was ascertained at specified time intervals until no such change (± 0.001 g) was observed [23]. The percentage of water uptake was calculated by Eq. 2.

$$\text{Water uptake} = \left[(w_f - w_i) / w_i \right] \times 100 \quad (2)$$

where w_f and w_i constitute the final and initial weights of samples, respectively (both in g).

2.13 Biodegradation in the soil

Biologically active soil of wood origin was made devoid of coarse fractions by sieving. Its moisture was ~54%, while the exchange capacity (pH_{KCl}) value equalled 6.9 and the content of organic solid phase carbon amounted to $16.9 \pm 1.36\%$. An automatic TOC analyser was employed in the experiment (TOC-LCSH/TOC-SSM, Shimadzu Corp., Japan).

In agreement with a study by Šerá et al. [25], a respirometric test was performed that applied a modified standard ISO 17556 [26] in 500ml flasks with septa in the cap. Each one contained 15 g of soil, polymer samples (50 mg), perlite (a heat expanded aluminosilicate, 5 g) and mineral medium (10 ml). Head space gas was sampled through the septum with a gas-tight needle and conducted through a capillary into a gas analyser (UAG, Stanford Instruments, USA), whereby the concentration of CO_2 was determined. The flasks were stored at 25°C and checked once a week initially, then every 14 days. The test was conducted in triplicate, with three parallel flasks containing identical samples, alongside four blanks. [25]

The fundamental criterion for biodegradability concerned a ratio of CO_2 , i.e. the amount produced during microbial breakdown in comparison with a theoretical quantity ($ThCO_2$). This was given by the balance of carbon present in the sample (Table 1) and expressed as D_{CO_2} (%), in accordance with Eq. 3 and Eq. 4 below.

$$ThCO_2 = w_{SAMPLE} \times TC \times (44/12) \quad (3)$$

Where $ThCO_2$ is the theoretical production of CO_2 from total substrate breakdown (mg), as determined by the balance of organically bound carbon in the tested film (TC in per cent divided by 100), and w_{SAMPLE} is the weight of the sample; 44 and 12 are the molecular weights of CO_2 and carbon, respectively.

$$D_{CO_2} = \left[(m_{SAMPLE} - m_{BLANK}) / ThCO_2 \right] \times 100 \quad (4)$$

Where m_{SAMPLE} is the quantity of CO_2 produced during the breakdown of the substrate (for the PHB and PHB-biochar films, in mg) and m_{BLANK} is the amount of CO_2 generated during the endogenous respiration of microorganisms (mg).

2.14 Mathematical models for the kinetic biodegradation process in soil

The courses of biodegradation over time for the extruded PHB film and those filled with untreated and chemically modified biochar, were described by three kinetic models, namely Keursten (I) [27], modified Gompertz (II) [28] and another based on a sigmoid function, as mathematically described by [29]. The various models are represented by Eq. 5, 6 and 7. The regression coefficients were calculated by applying the least squares method with a significance level of $p < 0.05$ in Statistica CZ 6.1 software.

The accuracy of the models was estimated graphically (see Figs. S6–S8) and then evaluated by determining their coefficients of correlation (R) and determination (R^2). Subsequent regression analysis showed consistent values of $R > 0.98$ and $R^2 > 0.98$.

Model I – Keursten model (first-order kinetics) [27]

$$D_{CO_2} = D_{max} \times [1 - \exp[-k \times (t - t_{lag})]] \quad (5)$$

Model II – modified Gompertz model [28,30]

$$D_{CO_2} = D_{max} \times \exp \left\{ -\exp \left[\frac{k \times \exp(1)}{D_{max}} \times (t_{lag} - t) + 1 \right] \right\} \quad (6)$$

Model III [29]

$$D_{CO_2} = \frac{D_{max}}{1 + \exp \left[2 + \frac{4k}{D_{max}} (t_{lag} - t) \right]} - \frac{D_{max}}{1 + \exp \left[2 + \frac{4k}{D_{max}} t_{lag} \right]} \quad (7)$$

where D_{max} is the regression coefficient representing the limit value in infinite time (%), k represents the biodegradation rate (in days⁻¹), t stands for time (days) and t_{lag} denotes the shift on the time axis that expresses the lag phase (days).

2.15 Biodegradation in river sediment

Water and sediment were collected from the river Olsava (Czech Republic) at the source of the stream, equating to quality class I according ČSN 75 7221 [31].

The test essentially adhered to ISO 19679 [32], albeit modified and optimized for the river sediment and laboratory closed respirometer employed, a MicroOxymax CO₂/O₂ unit fitted with an IR detector for CO₂ detection in gas phase (Columbus Instruments, Ohio, USA).

The testing medium was based on solid and liquid phases, the former being the river sediment (25 g wet mass), which fell to the base of a bottle (with a lid, 100 ml) upon being added into it; the liquid phase constituted a column of natural river water (30 ml) that was poured onto the sediment (the total volume of such solid matter and liquid in each container equalled 50 ml). After a 24-hour acclimatization of the river biocenose (25 ± 1 °C), a sample of the neat PHB film or one filled with untreated or chemically modified biochar was put into a bottle, where it settled on the top of the sediment layer, remaining at this level between the solid and liquid phases. This experiment simulated an object being submerged until finally reaching the bed of a river. The bottle-based systems were contained in a closed respirometric flask. Conducted in triplicate for every polymer material investigated, each bottle constituted a bioreactor, while positive references and 3 blanks (endogenous respiration) also underwent testing. The aforementioned reference specimens comprised cellulose filters that had been washed three times with boiling distilled water and dried at 105°C for 2 hours prior to use. The bioreactors were kept in a controlled-temperature chamber at 25 ± 1 °C under aphotic conditions. The primary biodegradability criterion concerned a ratio of CO_2 , i.e. the amount produced during microbial breakdown compared to a theoretical quantity (ThCO_2) and expressed as DCO_2 (%), in accordance with Eq. 3 and Eq. 4.

2.16 Fluorescence microscopy (live/dead bacteria)

Once extracted from the bioreactors for testing purposes, the specimens were rinsed with distilled water, placed on a slide and stained with a solution of laboratory-prepared fluorescent dye (a combination of SYTO®9 dye and propidium iodide) for 30 seconds. After any excess dye

was removed, the samples were rinsed with distilled water and studied on an Olympus BX53 fluorescence microscope (Olympus, Japan). SYTO®9 expresses an excitation maximum at 480 nm and propidium iodide at 490 nm. These wavelengths were discerned by applying excitation filters for SYTO®9 dye (no. 3) and propidium iodide (no. 5). Microorganisms stained with the former were denoted as alive (green), whereas those coloured with the propidium iodide dye were considered dead (red). Investigation of the images took place in cellSens software.

2.17 Sequencing analysis of the microbial communities present during biodegradation in soil

Specimens of the PHB and PHB-biochar films and blanks were sampled during the soil burial test. DNA was isolated with a commercial set, the DNeasy PowerSoil DNA extraction kit (Qiagen, USA), and underwent sequencing (SEQme s.r.o., Czech Republic). Specific regions were amplified, those corresponding with rRNA genes for fungi ITS2 (18S) and bacteria V3–V5 (16S), utilizing the primers F357 (5'-CCTACGGGAGGCAGCAG-3') and R926 (5'-CCGYCAATTYMTTTRAGTTT-3'), or ITS3F (5'-GCATCGATGAAGAACGCAGC-3') and ITS4R (5'- TCCTCCGCTTATTGATATGC-3'), respectively, with DNA barcoding and universal overhangs. Illumina adaptors were introduced in the second PCR, in accordance with normal directions for their use [33]. The products were evaluated by agarose electrophoresis, quantified with a fluorimetric AccuGreen™ High Sensitivity dsDNA Quantitation Kit (Biotium Inc., CA, USA), purified with NucleoMag NGS Clean-up and Size Select (MACHEREY-NAGEL, Germany) and pooled into a library. Sequencing occurred on a MiSeq unit (Illumina,

CA, USA), running the v2 reagent kit, with reads of paired-end 250 nt in an external laboratory (SEQme s.r.o., Czech Republic).

2.18 Bioinformatic processing and statistical analysis of Next-Generation Sequencing (NGS) data

Data processing and statistical analyses were performed using freely available software, R version 3.6.1. (R_Core_Team, 2020). The data gathered from the sequence analysis of the soil microbiome were processed with the DADA2 pipeline [34]. Taxonomy was assigned for the bacteria according to the SILVA 132 SSU NR 99 reference database [35] and the 8.3 release of the UNITE reference database [36] for fungi. The taxa count data sets obtained were further processed and visualized in the Phyloseq R [37] and Microeco [38] R packages.

*2.19 Growth test (*Triticum aestivum*) – pot trial test*

Certified seeds of *Triticum aestivum* were purchased from the ecological agricultural company Z. S. Pitín, a.s. (Czech Republic). Preliminary incubation revealed that all the seeds utilized in this study showed a rate of germination exceeding 90%. A two-stage stepwise experiment (Fig. S1) was designed to evaluate the impact of degradation fragments of the extruded PHB and PHB-biochar films on the germination and growth of the plants.

The first stage comprised a biodegradation experiment (soil burial test). Trials were conducted in 200-ml, self-watering, polypropylene cultivation pots filled with 10 g of water-saturated perlite

(the bottom layer) and a mixture of natural soil and perlite at the ratio of 1:2. Perlite (a heat expanded aluminosilicate) was supplemented to enhance aeration of the soil and the amount of water retained. PHB films in the form of test pieces (1.5×4 cm) were placed in the soil such that at least 1 cm of earth lay above and below the sample. The experiment was carried out in an aerobic environment at 25 ± 1 °C, under a controlled moisture of approximately 55%.

The second stage of the pot trial test related to plant cultivation. After specific intervals (10, 30 and 60 days of biodegradation of the polymer films), *Triticum aestivum* seeds (30 in total) were sown in pots that contained remnants of the PHB films, at a height of ca 0.5 cm above the degrading samples. Proper conditions were maintained to guarantee optimal plant growth and development, including the soil water content (approx. of 70% of the water-holding capacity), a temperature of 25 ± 1 °C and a light intensity of ca 7000 lux (16-hour day and 8-hour night system) [39]. Such humidity was controlled and the water content regulated during the experiment. Variable rotation of the pots occurred once every 3 days, and no fertilizers were utilized. The number of seeds that germinated were counted during the growth test.

The cultivation test of the *Triticum aestivum* plants lasted for 12 days. Upon completion of this period, the heights of the seedlings were determined prior to their removal from the pots, followed by gently cleaning to get rid of the earth and subsequent rinsing with distilled water. Weights were separately determined for the above-ground portions and roots (at an analytical level to the precision of 5 decimal places), while their dry masses were gauged after the plants had been oven-dried at 70°C to the point of constant weight.

3. Results and Discussion

3.1 Characterization of the modified biochar

The various forms of untreated and chemically modified biochar were characterized by X-ray fluorescence (XRF) to investigate their inorganic elemental composition. This revealed that no significant changes had occurred within the composition of samples treated with H₂O₂ or MA; hence, the untreated specimens and those modified with the aforementioned substances contained Fe, Ca, P, Si, K, Al and S. In contrast, the biochars that underwent modification with HCl actually retained the Cl, indicating the HCl had not been totally removed during the washing process with distilled water. The HCl solution affected the biochar by significantly reducing the amount of P present. In the literature Kopp et al. [40] stated that acidification increased the solubility of P and primarily solubilized Ca-associated P [40]. Herein, the belief was that this solubilized form of P was removed in the washing process.

Scanning electron microscopy (SEM) enabled the morphology of the biochars to be characterized, the subsequent micrographs in Fig. S2 showing the effects of the acidification and peroxide treatment. The biochar derived from sewage sludge possessed rough granular structures stemming from the complex components and relatively high quantity of ash they contained [41]. The untreated biochar exhibited a porous surface with irregular cavities (Fig. S2) and dispersed particles of inorganic components (diatoms). Studies by Zhang et al. [42] and Wang et al. [43] had given the impression that chemical modification would significantly reduce the amounts of ash and pyrolyzed by-products on the surfaces of the biochar specimens, thereby exposing portions of their original porous structures. Acidification or peroxide treatment failed to produce this effect, however, and no real deviation from the untreated biochar was apparent (Fig. S2).

XRF analysis indicated that the exterior agglomerates pertained to acid or peroxide residues that remained after the washing process stage (with distilled water) [41].

The pH values of the biochar samples (0.4% suspension in distilled water, 24 hours) dropped upon treatment with the HCl, MA or H₂O₂. A reason for this could have been insufficient removal of these substances by washing, although the chemical modification of the biochar surfaces was also potentially responsible. The biochar suspensions showed a drop from pH 7.377 ± 0.002 (for the untreated sample) to 3.592 ± 0.001 and 3.230 ± 0.006 for the HCl and MA treated specimens, respectively; in the case of the latter, it would appear that the biochar was carboxylate functionalized. Hydrogen peroxide, essentially a weak acidic oxidant, only diminished the pH level to 4.920 ± 0.001, probably through a rise in surface-level, weakly acidic carboxyl groups amount [22]. The decreases in pH reported herein, however, were likely caused by a combination of both factors (see the FTIR spectra in Fig. 1).

3.1.1 Attenuated Total Reflectance Infrared Spectroscopy

The functional groups in the untreated and chemically modified biochars were identified by FTIR analysis, as detailed in Figs. S3 and 1.

The FTIR spectrum for the untreated biochar presented in Fig. S3 shows a broad band at ca 3600-3000 cm⁻¹ pertaining to O–H stretching of the hydroxyl group, as well as potentially a mineral-based hydroxyl group related to silicon [44]. That at 1600 cm⁻¹ is associated with an aromatic C=C stretching vibration, while the one at ca 1400 cm⁻¹ relates to an aromatic C=C ring stretching vibration [45]. The broad band with the peak at 1020 cm⁻¹ results from the bending of

C–O, P–O and Si–O–Si groups [46]. The shoulder-like increment at 876 cm^{-1} could signify an out-of-plane ring bend of CO_3^{2-} [47].

Fig. 1.

The FTIR spectrum for the MA-modified biochar is given in Fig. 1. In this context, Li et al. [48] report that the band for the carbonyl group from the ester at 1703 cm^{-1} expresses the chemical modification of biochar. The bands at 1573 and 1354 cm^{-1} are characteristic for carboxylate asymmetric and symmetric stretching bands, respectively [48]. The rise in intensity at $3600\text{--}3000\text{ cm}^{-1}$, following the chemical modification process, indicates that parts of –OH groups are involved in the esterification reaction (Fig. S3). Thus, it was concluded that maleic anhydride had been successfully introduced on the surface of the biochar.

In agreement with Silber et al. [45], FTIR analysis of the HCl treated biochar revealed that no significant structural changes had occurred to it as a result of such treatment, merely small differences were evident instead. Comparing its spectrum with that for the untreated biochar, this acidified specimen shows a slight increase in the aromatic carbonyl/carboxyl C=O stretching band at 1703 cm^{-1} (a shoulder band), along with a decrease in one for the aromatic C=C ring at ca 1400 cm^{-1} . [45] A variation was observed in the content of CO_3^{2-} , however, whereby a peak signifying the antisymmetric out-of-plane ring bend of it could not be identified.

FTIR also detailed changes in the functionality of the H_2O_2 modified biochar, in agreement with Huff et al. [22]. Comparing the spectra for the untreated and given specimens revealed that these primarily occurred in the region of $1800\text{--}1200\text{ cm}^{-1}$, as detailed in Fig. 1. Treatment with H_2O_2 triggered the formation of acidic functional groups on the surface of the sample,

heightening the presence of oxygen-containing functional groups. It is known that biochar becomes hydrophilic when such groups are plentiful [42], a phenomenon which might prove critical to interactions between a PHB-biochar material and the crystallization mechanism of PHB [49].

3.1.2 *X-ray diffraction analysis*

The XRD spectra for the untreated and chemically modified biochar samples vary (see Fig. 2), suggesting that the modification processes induced different mineral crystals in them. The results mirror those of Zhou et al. [50], with the untreated biochar exhibiting characteristic peaks for SiO_2 at $20.9^\circ 2\theta$ and $26.6^\circ 2\theta$. As usual, peaks for CaCO_3 and graphite carbon appear at $29.4^\circ 2\theta$ and $26.6^\circ 2\theta$ [50], respectively, alongside another for carbon at $42.5^\circ 2\theta$ [50]. Evidence also exists for crystalline and semi-crystalline residual inorganic phases in the untreated biochar, visible at the limit of detection for XRD; these pertain to minerals and metal impurities (e.g. Al, Ca, Fe and Si) on the surface of the biochar (in agreement with the XRF analysis).

An aspect missing from the spectra for all of the chemically modified biochar samples was a clear peak at $2\theta = 29.4^\circ$, attributable to CaCO_3 . It is reasonable to assume Ca remained in the specimens that had undergone acidification or oxidation (see the XRF data). In this regard, modification could have led to the consumption of CaCO_3 or, alternatively, its conversion into an amorphous phase, as described in the FTIR section [51]. The hydrochloric acid treatment helped remove impurities and stabilize the chemical structure of the carbon skeleton of the biochar.

Fig. 2.

3.2 Characterization of the PHB-biochar films

The novel formulations described herein (Table 1) can be processed by melt blending and thermocompression. These techniques give rise to films that differ in macroscopic and microscopic appearance, depending on the type of biochar applied (Fig. S5).

Conducting a visual inspection revealed that incorporating particles of untreated or chemically modified biochar altered the colouring of the films, with variation from a yellowish shade (for extruded PHB) to hues of brown.

Scanning electron microscopy (SEM) was performed to investigate the surface morphologies of PHB films, these comprising an extruded sample and others containing untreated or chemically modified biochar. Supplementing the PHB matrix with a biochar induced roughness in the surfaces of specimens, as well as random particle distribution or agglomeration (BC-H₂O₂). Numerous cracks were even evident in the SEM image for BC-MA.

3.2.1 Characterization by polarized optical microscopy (POM)

Adding a filler has the potential to affect a polymer matrix with regard to its nucleation, microstructure, rate of crystallization, transcrystallinity, orientation and sizes of crystallite and spherulite [52].

Fig. 3 presents the minimal aggregation of biochar observed upon loading the PHB with 1 wt % of untreated or chemically modified biochar particles, the majority of which were separately and randomly dispersed in the biopolymer and lacked a contact network.

In agreement with Alghyamah et al. [53], the films filled with untreated biochar (BC) and acidified biochar (BC-HCl and BC-MA) possessed nuclei and spherulites. Dissimilar to the formations in the neat extruded PHB, they instead exhibited numerous tiny spherulites (see Fig. 10, section 3.3.1), far exceeding the quantity in the neat specimen. This crystallization in the blends could be attributed to heterogeneous nucleation initiated by the untreated or acidified biochar particles, preventing homogeneous nucleation of the PHB and giving rise to such crystallites with PHB spherulites that possess fracture (imperfect) morphologies. The findings of this investigation of spherulite morphology are generally in alignment with those obtained by DSC (Table 2), wherein the nucleation rate of the PHB was heightened in the filled specimens. The biochar particles also served as a nucleating agent for the PHB matrix, in turn causing the rate of crystallization for PHB to increase [53].

POM analysis (Fig. 3) revealed the existence of a high number of large crystalline structures in the film modified with peroxide treated biochar (BC-H₂O₂), in stark contrast with the extruded PHB. This phenomenon was associated with the slower rate of growth for spherulites in the presence of oxidized biochar particles. The result was the formation of sizeable PHB spherulites with a perfect morphology, i.e. resembling a Maltese cross [49]. In the literature Wang et al. [54] and Pustak et al. [52] state the speed at which spherulites appear in a polymer matrix is influenced by interfacial adhesion, the latter being altered by treating the surface of filler. The same authors also propose that inhibiting the movement of polymer chains by particle-matrix interactions might diminish the rate of spherulite growth.

POM also demonstrated the prevalence of interspherulitic accommodation of peroxide treated biochar particles in the PHB, which could not be engulfed by spherulites, as particles of untreated or acidified biochar. However, such a phenomenon failed to explain if these

microparticles were ejected to the surfaces of the spherulites or whether they ceased the growth of the latter, regardless of the capacity for nucleation [52]. This was probably caused by the hydrophilicity of the H₂O₂ treated biochar (see the FTIR section). The hydrophilic nature of the H₂O₂ treated biochar was not compatible with the highly hydrophobic PHB, which contributed to poor particle dispersion (see the SEM for the films) [42,52]. Alternatively, the H₂O₂ treated biochar contained unreacted peroxide that failed to be removed by the washing process, therefore the extrusion procedure had caused unstable active oxygen species to appear on the PHB surfaces, resulting in less predictable outcomes [55]. This finding was in agreement with the FTIR results, as no peak at 2854 cm⁻¹ for a symmetrical CH₃ group in the PHB was detected for the BC-H₂O₂ specimen (see the FTIR section). This functional group probably underwent the above-mentioned oxidation processes.

Fig. 3.

3.2.2 Atomic force microscopy (AFM)

As reported by Woolnough et al. [56] and Julinová et al. [23], the colonization of materials by microorganisms and the consequent formation of biofilms are affected by various surface-related characteristics, including roughness, wettability (hydrophilicity or hydrophobicity) and charge. The first of these examples influences the succession and diversity of the microorganisms, as reflected in the rate of biological decomposition [23]. Rough surfaces could prove easier to colonize, as cells in crevices are protected from adverse shear forces. Such unevenness also provides a greater ratio of surface area to bulk, promoting biofilm development [56]. Therefore, AFM was performed to gauge the roughness of the films and obtain complementary data on the distribution of biochar particles in the PHB matrix [23].

As detailed in Fig. 4, no major differences existed in the roughness (parameter Sa) of the extruded PHB film and those supplemented with the untreated or chemically modified biochars. Minimal variance was observed in this regard, merely 4–8 nm, meaning the surface wettability (see section 3.2.7, Fig. 8) and biodegradation of the enhanced materials were largely unaffected by this parameter. In relation to the proportion of filler present, phase-contrast imaging revealed that the blends differed slightly from each other (Fig. 4). The amount of filler at the phase boundary ranged between 7% and 11%, such small changes in the content of biochar being calculated by determining the surface energy of the dispersed particles with respect to the carrier matrix. The parameter of roughness did not correlate with other trends for surface wettability or biological degradation, consequently it was deemed that no dependence existed between distribution of the biochar particles on the surfaces of the films and the biodegradability of the latter.

Changing the phase angle rendered the tonal differences evident in the phase images below, ranging from the lighter ones denoting a hard crystalline phase to the darker pictures representing a soft amorphous phase [57]. This finding was significant with regard to colonization of the film surfaces by soil microorganisms and the initial stage of biological decomposition (see section 3.3.1, Fig. 10).

Fig. 4.

3.2.3 *Attenuated Total Reflectance Infrared Spectroscopy*

The FTIR spectra for the tested films are presented in Figs. 5a and 5b. The characteristic absorption bands visible for PHB (Fig. 5a) are attributed to CH₃ (2976, 1452, 1379 cm⁻¹), CH₂ (2931 cm⁻¹), C=O stretching (1720 cm⁻¹) and C–O–C stretching (1180 cm⁻¹, 1130 cm⁻¹). No major changes in PHB structure are presented in Fig. 5a, since significant interactions did not occur among the components. The presence of biochar particles is demonstrated in Fig. 5b by a shift and alteration in the intensity of absorption bands at 3000-2840 cm⁻¹ [58]. Variance is also evident in the spectrum for the BC-H₂O₂ film: i) the adsorption band at 2931 cm⁻¹ for the stretching vibration of the asymmetric CH₂ group of a monomer chain appears at a higher value; and ii) the peak at 2854 cm⁻¹ for the symmetrical CH₃ group, a consequence of crystallization with a conformational composition [59], is not apparent. These changes suggest that a chemical interaction transpired between the H₂O₂ and PHB, thereby altering the helical polymeric and crystalline structure.

It is known that PHB has a narrow processing window and is prone to thermal degradation during processing. Such degradation is usually catalysed when fillers are present, it gives rise to localized hotspots which heighten the temperature of the process through internal friction [60-63]. The authors Maiti & Batt [61] investigated PHB-based nano-biocomposites reinforced by montmorillonite. They discovered that the presence of aluminium Lewis acid sites in the silicate layers promoted the thermal degradation of PHB, wherein catalysis was induced by the hydrolysis of ester linkages. Haelderms et al. [63] reported that supplementing samples with biochar led to a reduction in their molecular weight, since processing composites in the presence of solid particles raised the level of shear stress, with friction causing localized zones to overheat. They determined that temperatures potentially exceeded 180°C in such hotspots, as a consequence of which PHB underwent quantitative conversion, primarily into crotonic acid (at

225-250 °C). Moreover, the biochar particles could have heightened mechanical forces on the PHB, contributing greatly to its decomposition. Inorganic oxides (e.g. CaO, MgO and Al₂O₃) on the surface of biochar might constitute another reason for this twofold loss in molecular weight of PHB. They have been shown to destabilize PHB during processing, leading to much easier formation of volatile degradation products [60].

The usual trend is for pure PHB to undergo thermal degradation during extrusion [64], initiated by a six-membered ring transition that forms carboxylic acid and unsaturated groups. Corresponding bands arise at 3437 cm⁻¹ and 1629 cm⁻¹, characteristic of increases in hydrogen-bonded groups and C=C bonds, respectively. However, the FTIR spectra for the novel films tested herein do not possess an absorption band at 1629 cm⁻¹ (Fig. 5a), merely a hint of one at 3436 cm⁻¹. This suggests that minimal thermal degradation occurred during the preparation of the films, due to the presence of the biochar particles; hence, its influence on the course and degree of biodegradation can be excluded.

These favourably findings supported the application of additives such as neat or chemically treated biochar, wherein elements (e.g. Fe, Ca and Al), acids (HCl and MA) or peroxide are found.

Fig. 5.

3.2.4 X-ray diffraction analysis (XRD)

The XRD patterns for the extruded PHB and biochar supplemented films are presented in Fig. 6. Several peaks are visible at 2θ for the neat material, attributed to crystalline phase regions in poly-3-hydroxybutyrate.

In agreement with Iulianelli et al. [10], the diffractograms evinced that the samples had a semi-crystalline profile, presenting peaks corresponding to orthorhombic crystal planes. Two strong peaks of scattering intensity at ca $2\theta = 13.37^\circ$ and 16.8° were assigned to (020) and (110) of the orthorhombic unit cell with helical chain conformation, respectively. Other reflections were observed at ca $2\theta = 16.31^\circ$, 20.08° , 21.56° , 22.65° , 25.54° and 27.20° , corresponding to (011), (021), (101), (111), (121) and (040), respectively [10]. In addition to the orthorhombic α -form crystals of such conformation, the PHB films also possessed a small amount of β -form ones with zigzag conformation, as denoted by the diffraction hump for 2θ at 20.08° . Since β -form crystals were present, the indication was for a heightened level of molecular stretching in the amorphous regions between the α -crystalline lamellae.

The crystalline structures of the filled PHB films were not altered to the extent that the biochar in them affected the crystalline phases of the PHB, while the crystallinity of the films was mostly conferred by the parent polymer. The peak at $2\theta = 26.9^\circ$ confirmed the specimens contained biochar particles, attributable to inherent crystalline carbon or quartz (SiO_2); see Fig. S4 [46]. The intensity of this peak vary in accordance with the distribution of particles in the films. It was also seen, that the maximal intensity of all peaks to be weaker for the filled samples. The causes for this were an increase in the content of the amorphous phase on the films surface (see the AFM section) [65]. The relative population of the (020) crystal plane to (110) plane was reversed in the BC, BC-HCl and BC-Ma films, implying that different, preferred routes for crystal growth were followed [66].

Fig. 6.

3.2.5 *Differential scanning calorimetry*

In order to investigate the effects of the various biochars on crystallinity, DSC analysis was conducted on the neat and filled PHB films (Table 2). The results indicated that the transition temperatures T_m and T_c remained largely unaffected. The data revealed that the T_c for the filled films slightly increased, according to the type of biochar incorporated. The maximal change in T_c was recorded as ca 4%, in comparison with the extruded PHB. A 10% increase in values for crystallinity was observed for BC-HCl and BC-MA (Table 2), compared to the reference sample. Taking into consideration the XRD findings (see Fig. 3; pH values for aqueous suspensions of the acidified biochars), it would appear that crystalline compounds not removed at the washing stage, such as HCl and MA during the fabrication process, were responsible for the aforementioned rise in crystallinity. It is probable that the films filled with the untreated biochar or modified forms with HCl or MA possessed heterogeneous nucleation sites, hence they required less undercooling for PHB to crystallize, suggesting the biochar particles had a nucleating effect on the biopolymer. This phenomenon was evident in the polarized optical micrographs (Fig. 3), wherein the BC-HCl and BC-MA films contained an abundance of nuclei, unlike the pure extruded PHB sample.

Table 2

3.2.6 *Thermogravimetric analysis (TGA)*

Thermogravimetric analysis was carried out to discern the thermal stabilities of the tested films. Thermogravimetric curves for the samples across the temperature range of 240-340 °C are given in Fig. 7.

All tested films presented a very similar temperature for the onset of the degradation process, varying only by ca 1%, and little disparity was also seen in the maximal values (T_{max1} ; see Tables 3 and 4 for details). With regard to total residual mass, the least (1.06%) was recorded for the untreated biochar specimen, with BC-H₂O₂ at the other extreme at 2.13%, this constituting a difference of +79% compared to the pure extruded PHB.

Table 3

Table 4

Fig. 7 present the TG and DTG curves obtained. From the former (Fig. 7a), a single degradation step was evident for the tested compositions, with DTG (Fig. 7b) revealing that it transpired in two secondary stages (see the double peak). The position both of maxims is very similar. Most samples manifested a slightly higher intensity in the latter of the two peaks, whereas BC-H₂O₂ exhibited this in the initial one, an aspect potentially connected with residual peroxide or associated peroxide bonds that enabled oxidation at a reduced temperature. Changes in mass for the primary degradation process varied from ca 98.3-99.9 %, a difference of ca 1% compared to the reference sample.

It was concluded from the TGA analysis that the biochar, in untreated or modified form, did not significantly influence the thermal stability of the tested compositions. This finding is in

agreement with Haelder et al. [63], who stated the temperature at which PHB/char composites started to degrade was only very slightly affected by the presence of biochar particles (to the amount of 40 wt%). It was also deduced that the BC-H₂O₂ would cause a greater amount of ash to be generated upon its thermal degradation, as a consequence of the peroxide treatment it had undergone.

Fig. 7.

3.2.7 *Surface wettability*

As defined in the literature, analysing the water contact angle (WCA) of a material enables its surface wetting behaviour to be determined. Such an investigation pertains to microorganisms, respectively the actions of their cells, including attachment, growth and proliferation. Hydrophilic substrates are required for cell adhesion (biofilm formation), yet excessive hydrophilicity can result in cell detachment [67]. The chemical nature of the tested surface is important, although physical characteristics also affect WCA values.

As described by Dhania et al. [68], a surface is considered hydrophilic, hydrophobic or super hydrophobic, for which water contact angles equal $<90^\circ$, $>90^\circ$ and $>150^\circ$, respectively. As detailed in Fig. 8, the WCA for every PHB sample was less than 90° , thus their surfaces were deemed to be hydrophilic. Researchers have reported that a WCA of 40° to 70° is optimal for a biodegradable material [67].

The water contact angle for the extruded PHB measured 61.00 ± 0.80 degrees, while the values for BC and BC-HCl were 62.27 ± 3.53 and 64.63 ± 0.95 , respectively, so little difference

existed between them. In contrast, the WCA for the BC-MA and the BC-H₂O₂ films equalled 71.12 ± 2.40 and 78.20 ± 2.01 degrees, respectively (Fig. 8).

The MA-treated biochar in the former of the two could have been responsible for this behaviour (see the FTIR for the biochar in Fig. 1) through interaction hydroxyl groups with PHB chains. As a consequence, the orientation of these groups did not affect the chemical properties of the surface, thereby heightening the hydrophobicity of the material. Holešová et al. [69] stated that polymer films with different sizes of spherulite grains could exhibit raised WCA values. The surface of the BC-H₂O₂ film was completely covered in PHB crystallized spherulites (resembling a Maltese cross). They had the effect of restricting the interactions of water molecules and polymer chains, and possibly even rendered it a non-polar surface. The sample had low free energy and a heightened contact angle.

An increase in hydrophobicity might be an undesirable characteristic, however, as it limits the exposure and availability of a surface to microorganisms. It proves favourable, though, when materials are subjected to conditions of high relative humidity, e.g. in packaging applications.

Water adsorption by polymers is consistent with established mechanisms for their degradation, where penetration by extracellular depolymerase enzymes leads to chain cleavage and preferential erosion of amorphous regions [56]. In the same study, Woolnough et al. [56] states that water contact angles only pertain to the surface and not the bulk hydrophilicity or hydrophobicity of the given polymer. Gravimetry was conducted herein to determine the latter aspect, revealing the water absorption of the films was very low, just 0.11 ± 0.31 % for the extruded PHB, 0.25 ± 0.19 % for BC, 0.13 ± 0.11 % for BC-HCl, 0.17 ± 0.10 % for BC-MA and 0.29 ± 0.20 % for BC-H₂O₂. This analysis occurred upon completion of a 12-day uptake test (55% humidity; see Table 1).

On the basis of the wetting and adhesion interactions observed between the tested specimens and water, it was concluded that the biological degradation of the films was not significantly influenced by the hydrophilicity of their surfaces.

Fig. 8.

3.3 Biodegradation of the PHB-biochar films in agricultural soil

From an ecological and financial perspective, the novel PHB materials supplemented with biochar could prove appropriate in the manufacture of biodegradable plastic mulch. Such a product is tilled into soil, and can be removed and composted on-site following its usage. Consequently, it was important to evaluate them with regard to their degradation in the intended environment, the ultimate aim being to avoid the unnecessary accumulation of plastic.

The biodegradation curves of the films are presented in Fig. 9, wherein the extent to which the microcrystalline cellulose (the reference material) had biodegraded exceeded 80% by the close of the experiment (with a lag phase of 5.2 ± 0.6 days), indicating the test was valid.

The polymer samples underwent biodegradation after a lag phase of between 14 and 25 days (according to the given type); the latter constituted the time needed for microorganisms to adhere to such surfaces. All of the specimens exhibited a linear trend throughout the incubation period of 5 months, as reflected in their biodegradation curves. This suggests a surface erosion mechanism predominated in the first and second stage of the experiment [70].

The extruded PHB degraded by 86.52 ± 14.59 % in 7 months, following a lag phase of 17.0 ± 7.2 days, confirming it is a highly biodegradable polymer. Great variations were observed

between the triplicates, common in biological activities involving soil. The filled films all decomposed more slowly, the differences highlighting their levels of resistance to biodegradation.

The findings suggest that the untreated and chemically modified biochars greatly contributed to delaying the full biodegradation of the PHB films, in agreement with Merino et al. [71] and She et al. [72]. The latter authors attributed the slower biodegradability of composites supplemented with “natural biochar” to the hydrophobic character of the biochar, which establishes an environment that delays the growth of microorganisms. It was observed herein that every sample had the optimum hydrophilicity for biodegradable materials (see Fig. 8). The assumption was made that in the PHB and untreated biochar specimen (lag phase 14.3 ± 6.4 days) biodegradation of the surface amorphous phase transpired and then ceased, whereupon microorganisms became immobilized on the surface of the biochar. The latter has a well-developed pore structure and provides a suitable habitat for microorganisms, while the mineralizable organic matter and inorganic nutrients within it could also promote microbial growth [73]. This is consistent with the SEM observations for the BC film. As detailed in Fig. 11, following the breakdown of the amorphous phase, the biochar particles became available to soil microorganisms and were subsequently colonized by bacteria, leading to their immobilization [74]. The number of active microorganisms participating in the biodegradation of the amorphous phase was reduced as a consequence, including in the interlamellar space of the PHB spherulites. In this case, retardation of the biodegradation of the BC film fell in extent from 86% to 65% (64.39 ± 12.98 %).

Fig. 10 shows that the PHB film filled with acidified or oxidized biochar did not exhibit colonization of its biochar particles by microorganisms after the amorphous phase had

decomposed. According to Yu et al. [73], pH has the capacity to affect bacterial growth and change the metabolic rate and production of extracellular polymeric substances (EPS) by influencing the metabolic pathways. In general, a pH of 6–8 favours the development and activity of most bacteria, whereas a strong acid or base diminishes bacterial metabolic action and subsequently destroys fixed cells; therefore, the ability of bacteria to bind to biochar is also lessened. In a strong acidic medium, hydrogen ions alter the charge balance on the surface of a cell and the permeability of its membrane, thus preventing fixed cells from obtaining adequate nutrients. In a strong alkaline medium, protein denaturation and cell death may occur, resulting in a drop in EPS production [73]. The belief is that, as a consequence of such phenomena, the biodegradation of BC-HCl and BC-H₂O₂ was significantly inhibited. BC-HCl achieved 37.02 ± 8.17 % mineralization after 7 months with a lag phase of 25.0 ± 6.5 days. This could have been due to the relatively high amounts of protons (H⁺, H₃O⁺) in the porous biochar. BC-H₂O₂ showed a value for mineralization of 55.90 ± 0.63 % after 7 months, with a lag phase of 14.8 ± 5.4 days, as acidic functional groups had appeared on the biochar surface. Since maleic anhydride is a highly biodegradable compound, acidifying the biochar did not exert a major effect on the biodegradation of the film. BC-MA achieved a percentage of mineralization of 71.63 ± 7.67 % after 7 months (lag phase 16.0 ± 2.6 days).

Fig. 9.

The experimental (absolute) results in Table 5 confirm the hypothesis above that adding biochar inhibits the rate of biodegradation of PHB.

Evaluating the retardation by the untreated and chemically modified biochars on the biodegradation of the PHB materials involved modelling cumulative biodegradable curves based on three functions: a. the first-order Keursten model (I) [27,75], applied to highly biodegradable materials; b. modified Gompertz (Model II) [28,30], enabling consideration of the lag phase (absent from Model I); and c. Model III, as described by Rial et al. [29], applicable for compounds with a concentration-dependent inhibitory effect. All of the kinetic models above relied on assumptions about decreases in substrate concentration and product formation based on carbon dioxide evolution.

The results of such kinetic modelling of biodegradation, founded on experimental data, are presented in Table 5. The correlation coefficient (R) and coefficient of determination (R^2) parameters were applied to validate the findings of the models, as detailed in the Table 5. Each model was an excellent fit ($R > 0.99$) for the observed data, although none of them proved ideal for describing the biodegradation kinetics of every PHB material. A potential reason was that accurate assessment of the concentration of soil microorganisms (biomass) and the residual polymer in the earth was needed for such modelling [76].

The most common model (I) generated a convex curve that was optimal for microcrystalline cellulose (the reference material). It depicted the rapid production of CO_2 at the initial stage of incubation, a subsequent gradual slowdown and then a constant slight increment (its plateau) at the close of the experiment. For the tested samples, model I failed to provide any meaningful values for D_{max} and constants, though, in agreement with Calmon et al. [77]. Model II was accurate according to R and R^2 , yet it proved inadequate at relevantly predicting the sigmoid shape (t_{lag}) of the experimental data for the extruded PHB, BC and BC-MA specimens, even though the lag phase was incorporated in calculations [78]. The kinetic model that fitted the

experimental data the best was III, except for the BC-H₂O₂ sample. Designed by Rial et al. [29], primarily for evaluating the influence of toxic metals on microorganisms, Model III indicated that the untreated biochar particles and those modified with HCl exerted an inhibitory effect on the biodegradation of PHB.

In summary, the rate of biodegradability of the PHB materials with the untreated or chemically modified biochars took the following order: BC-MA > BC > BC-H₂O₂ > BC-HCl. Model III was capable of predicting that the rate of decomposition would diminish as the content of particles increased. This could prove crucial to designing and producing polymers with a controlled lifetime.

Table 5

3.3.1 Scanning electron microscopy and fluorescence microscopy

These techniques assessed changes in the morphologies of the film surfaces and in microbial colonization. Fig. 10 contains SEM images for the extruded PHB film and specimens supplemented with untreated or chemically modified biochar taken at 10, 30, 90 days and 5 months of biodegradation in the soil, as also detailed in Table 6.

Morphological changes are evident in every surface (prior to biodegradation, see Fig. S5), corresponding to cavities and structures, the latter are spherical (e.g. bacteria) and extended (e.g. fungal filaments and debris) in form.

It is known that microbial attacks commence at accessible enzymatic sites, such as the amorphous phase and chain ends at the edges of crystals [11,19,79]. AFM analysis revealed that the biochar, with respect to its properties, altered the phase composition of the PHB film

surfaces. Regarding the filled specimens, the relative content of the amorphous phase ranked in the following order: BC-HCl>BC-MA=BC>BC-H₂O₂. This finding corresponded to the extent of erosion and surface colonization by microorganisms after 10 days of testing.

The surfaces of the extruded PHB, BC, BC-HCl and BC-MA were strongly eroded at 30 days, with just a few areas of original, non-degraded material remaining. Pores had formed and the ongoing degradation had given rise to a very rough topography with an enlarged surface area, which stimulated colonization by microorganisms.

Upon 90 days of biodegradation, regular crystal structures and spherulites were observed, as detailed in Fig. 10. The filled PHB films exhibited significant differences in crystal geometry. For instance, BC-H₂O₂ possessed large spherulites and there was no evidence of crystal degradation. The amorphous phase seemed to be the only substrate that degraded during the first 150 days, a finding consistent with a previous study [19]; wherein it is reported that the morphology of a crystal structure (spherulites) exerts a significant impact on the rate and degree of biodegradation of the crystalline zone.

The nucleation of PHB crystals transpired through environmental processes in BC and BC-MA. This was caused by the plasticizing effect of water, which entered their matrices through the eroded surfaces, disorganizing the crystal structure of thinner crystallites [19,80].

Fig. 10.

Table 6

Fluorescent staining was applied to the extruded PHB film and filled biopolymer specimens to visualize the biomass on them. Subsequent fluorescent microscopy (Fig. S9) exposed changes in

microbial attachment to the film surfaces throughout the entirety of their biodegradation; the findings were in agreement with those of SEM.

Fig. S9 details the increase in microbes that had adhered to the extruded PHB over the 90-day period. The BC-MA and BC-H₂O₂ films demonstrated a lower level of such activity over the same time frame, probably due to the large spherulite structures present (see SEM at 90 days). In the case of the BC-HCl specimen, the HCl treatment that the biochar had received appeared to restrict or even prevent the accumulation of live microorganisms, thus significantly hindering degradation of the PHB. As the biofilm on it spread, the biological breakdown of the polymer matrix caused the HCl to be released from the biochar particles. This induced an antimicrobial effect and eventually the emergence of a partially dead layer of microorganisms. Live microorganisms were again discerned on the BC-HCl film at 90 days, though, indicating such biofilm growth was delayed rather than halted. Goodwin et al. [83] described the phenomenon as the formation of a protective layer of dead microorganisms.

Fig. 11.

3.3.2 Sequencing analysis of the microbial communities present during biodegradation in soil

On the basis of the SEM and fluorescence analyses (see Figs. 10 and S9), the conclusion was drawn that the initial phase of biodegradation (see Fig. 9) consisted of the following stages: a. biofilm formation, including decomposition of the amorphous phase; b. erosion of the surface and release of the reagents (HCl, MA or H₂O₂) from the biochar; and c. consequent inhibition of microbial growth (antimicrobial activity), causing prolongation of the lag phase and an associated reduction in the speed at which biodegradation transpires. It is known that the first

phase outlined above significantly affects the entire rate of biodegradation [19,75], hence the sequence analysis conducted.

The SEM findings obtained for the soil experiment (respirometric in type, see Fig. 9) informed a further biodegradation test with optimized intervals of sampling (14 and 21 days) capable of defining the biofilm more fully. The expectation was that gradual release of the reagents would alter the given community to some respect.

However, the results from this study suggest that the different biochar treatments in the polymer did not substantially affect the biofilm communities that colonized their surface (Fig. 12). After 14 days, it was evident that *Streptomyces* [84] and *Oxalobacteriaceae*, probably genus *Massilia* [85], were the major degraders of the polymer in our experiment and are well-known to possess suitable PHB depolymerases. Specifically, the porous structure of biochar provides a habitat for microbial colonization, which can lead to increased microbial diversity, including the potential enrichment of specific bacterial taxa. Here *Planococcaceae* [86,87] appeared on some materials containing biochar, which can also be related to their roles in organic matter decomposition and nutrient cycling. This group is also known to be equipped with PHB metabolizing enzymes [88]. Interestingly, the latter group was less present in the HCl-treated biochar sample, where the biodegradation was retarded. The same pattern could be observed with *Micrococcaceae* [89] potent degraders of many complex organic compounds, including PHB. At the second sampling time, after 21 days, the communities on different materials were even more similar, with an apparent expansion of *Xanthomonadaceae* and *Rhizobiaceae* presence.

Comparing Shannon and Simpson diversity indexes (Fig. S10), the HCl-treated samples stand out as having the lowest diversity. The limited number of taxa that were initially able to colonize

this material can be the reason for the more extended lag phase and the lower rate of the material biodegradation.

Fungi communities basically were very similar among the materials but also between the materials and the control soil experiments (Fig. 12 and S11). This suggests that although fungi are important contributors to PHB biodegradation, bacteria are probably crucial to initiating the process [90]. Taxa, already dominant in the soil community, also dominated the fungi community on the material surface. Fungi taxa previously identified as important for PHB biodegradation were also found here e.g., *Talaromyces* (the Aspergillaceae family, [91]) or *Fusarium* (the Nectriaceae family).

In conclusion, the results from sequencing analysis suggest that the different type of biochar present in the polymers did affect the biofilm communities that initially colonised each polymer type.

Fig. 12.

3.4 Environmental impact

3.4.1 Influence of the PHB-biochar films on a river environment

Even though PHB has been variously employed in an attempt to decrease synthetic plastic residues in terrestrial ecosystems, in addition to being touted as a viable alternative in a multitude of applications (e.g. in agricultural mulch films), associated biodegradation processes usually lead to it breaking up into micro- or nano-sized pieces of plastic; consequently, these could be dispersed and transported by surface run-off and enter an aqueous environment [92]. Since the

composition of a biodegradable material has the potential to affect natural aqueous microorganisms, it was important to discern the environmental impact of the types reported herein.

In this context, experiments were conducted on the biological degradation of the prepared films and their impact on a river environment. The results are detailed in Fig. 13, affirming that the microcrystalline cellulose (the reference material) had exceeded 90% biodegradation by the end of test, with a lag phase of 4.6 ± 3.9 days, thereby validating the test. The Fig. 13 also shows that the extruded PHB and biochar filled films degraded far more rapidly in water than in soil. An explanation for this was proposed by Wang et al. [93]. They suggest that PHB degradation transpires via a hydrolytic reaction of polyester, under the catalysis of PHA-depolymerase secreted by degraders; and since the latter is water-soluble, enzymatic degradation takes place more easily in an aquatic ecosystem.

The biodegradation of the tested samples commenced after a lag phase of between 4 and 12 days, according to the given type. The lag was associated with the following: a. the time needed for the microorganisms to adhere to the surface, possibly related to the hydrophilicity of the sample (see Fig. 8); b. the content of the amorphous phase on the surface (see the AFM analysis); and c. a combination of the two.

The extent of biodegradation demonstrated by the extruded PHB equalled 54.02 ± 2.36 % after 32 days, with a lag phase of 11.9 ± 1.9 days, denoting it as a highly biodegradable biopolymer. This was in agreement with Volova et al. [94] and Kadoya et al. [95], who reported 43.5% and 50% decomposition for PHB films in river sediment, respectively; under natural conditions at 20°C, and upon 42 and 30 days of testing, respectively [94,95]. The lag phase stated at the top of this paragraph, however, was the longest of all the tested films (11.89 ± 1.88

days). Since its WCA value indicated the material was indeed hydrophilic, the assumption was that such a lag time related to the high content of the crystalline phase on its surface (see the results for AFM). Fig. S12 shows that a dense biofilm matrix had formed on the PHB film by 22 days of incubation, its surfaces being completely coated in thick, compact matter [96] subsequently identified as diatoms. An initial colonizer of polymer film surfaces in rivers, these unicellular organisms contribute greatly to the formation of biofilm and its overall biogeochemical activity [97].

BC degraded by 64.6 ± 1.21 % within 32 days, its lag phase lasting 9.36 ± 1.41 days. Fig. S12 presents the dense biofilm matrix that had formed on its surface by 22 days of incubation. It was covered in a thick, compact biofilm and possessed an exopolysaccharide matrix [82]. No accumulation of microorganisms was evident on the biochar particles, unlike in the soil tests (see part 3.3.1, Fig. 11), thus its biodegradation was not retarded through microbes becoming immobilized.

The biodegradation recorded for BC-HCl amounted to $77.2 \pm 3.43\%$ after 32 days with a lag phase of 3.85 ± 1.07 days. River water has a high pufration ability, so it withstands the effects of acidification well. At the end of the respirometric test, the pH of the aqueous phase measured 8.006 ± 0.001 (Table S1). BC-HCl did not show any evidence of diatoms and biofilm formation (see Fig. S12), probably since the HCl leached from the biochar once the amorphous phase on the surface had biodegraded. Despite this, the BC-HCl specimen mineralized the fastest of all the tested films. In this context, Nauendorf et al. [98] experimentally verified that biofilm formation and degradation were not necessarily related. [98,99]

BC-MA behaved similarly to the extruded PHB, showing no notable difference in the rate or extent of biodegradation (50.31 ± 5.73 %). Its lag phase was shorter (8.73 ± 5.27 days), though, likely due to the greater amount of the amorphous phase on its surface.

The BC-H₂O₂ film had only biodegraded by 47.66 ± 10.43 % within 32 days, while its lag phase was lengthy at 9.94 ± 4.84 days. The hypothesis is that a synergetic effect was the cause, pertaining to the relatively high WCA (Fig. 8) and considerable content of the crystalline phase on the surface in the form of large spherulite structures (see the POM and AFM analysis).

In summary, the chemically modified biochar did not negatively impact the biodegradation of the filled PHB films in the river environment.

Fig. 13.

3.4.2 Screening test for phytotoxicity (Triticum aestivum)

Liwarska-Bizukojc et al. [100] report that the presence of biodegradable plastic (e.g. PHB or PLA) in soil variously affects the development of plant organs. Such plastic could inhibit or stimulate the growth of roots or stems, while no such effect may be evident at all. The key factors are the concentration of the plastic, its chemical composition and the species of plant [16,100].

A phytotoxicity assessment was conducted to investigate this. It permitted evaluation of what adverse effects would arise from acidification of the soil through the gradual release of the acid or peroxide from the biochars. The test involved degrading the films in an agricultural environment and gauging their influence of the growth of a major crop, namely *Triticum aestivum* (common wheat). The resulting data are presented in Table S2.

According to the Liwarska-Bizukojc [100], seed germination is largely independent of soil composition as inherent constituents are drawn upon instead [101].

Scrutinizing the results (see Table S2) revealed that the films probably influenced the roots of the plants, although the active reaction of the soil (pH/H₂O) amounted to 7.42 ± 0.024 for every sample at the close of the test [102]. The phenomena of inhibiting the growth of roots (BC-MA, after 10 days of biodegradation) or stimulating it (BC, 10 days) were most likely a consequence of changes that occurred in the physical and chemical properties of the soil in which the specimens were buried. Zhang et al. [16] declared this as due to the following: a. the presence of macro- or micro-sized particles of film; and b. the slow release of additives (herein acid or peroxide from the biochars). It is likely that the films influenced the soil in various ways, e.g. its density, pore space, moisture, evaporation and water retention [16]. Alterations of this kind could either benefit the given environment through better aeration or impact it via dryness or loss in moisture [100].

It was found that the tested films did not significantly affect the development of stems (length, the dry weight of biomass), hence no negative influence was exerted on the growth of the plants by their biodegradation in the soil [18].

Despite the positive results reported above for the screening test (without statistical assessment), further phytotoxicity experiments are necessary.

4. Conclusion

This study investigated the possibility of utilizing oxidized or acidified biochar as an environmentally-friendly antimicrobial agent. The conclusions below were based on the experimental findings.

(i) Technological summary

- Changes in the extent of the crystallinity of the films were instigated by the crystallinity of the respective biochar.
- The DSC results and POM analysis indicated that the particles of the untreated or acid treated biochars acted as effective nucleating agents for crystallization of the PHB matrix.
- The untreated and treated biochars did not significantly influence the thermal properties of the prepared mixtures with PHB.

(ii) Biodegradation summary

- The hydrophilicity of the polymer surfaces (as gauged by WCA) did not correlate significantly with the lag phase of biodegradation; moreover, other hydrophilic properties, such as water absorption, exhibited no real connection with the biodegradation kinetics.
- The PHB degraded at slower rate in the presence of the untreated or chemically modified biochars, indicating a dependency in this regard. Hence, a potential exists to regulate its natural rate of biodegradation by supplementing (1 %w) it with untreated or chemically modified biochar.
- The extent of initial surface erosion and microbial colonization depended on the phase composition of the surfaces of the extruded PHB film and samples filled with untreated or chemically modified biochar.

- Following the initial erosion of the surface, the form of the biochar present in the biopolymer influenced the biofilm communities that initially colonized it.

(iii) Environmental impact

- The chemically modified biochars exerted no negative impact on the biodegradation of the filled PHB films in the river environment.
- The *Triticum aestivum* plants did not exhibit any visible phytotoxic effects as a result of the biodegradation of the films. With respect to the bioassay performed, the film comprising PHB and the HCl treated biochar was observed to be biocompatible with soil.

This study shows that environmentally-friendly films capable of the adjustable and controlled release of additives (with an antimicrobial effect) can be efficiently produced through extrusion and thermocompression, without the need for expensive solvents or lengthy procedures. The process involved is quick and sustainable, hence both economically and environmentally beneficial. The novel PHB/acidified biochar material showed promise as a sustainable and flexible film suitable for agricultural applications.

Supporting Information

Schematic diagram for the growth test of *Triticum aestivum* in pots; SEM images of the untreated and chemically modified biochars; FTIR spectra for the untreated and chemically modified biochars; XRD diffractograms of untreated biochar (powder) and PHB filled with untreated biochar (film); Macroscopic photographs and SEM images of the PHB films; Kinetic analysis of the biodegradation of extruded PHB and PHB films filled with untreated or

chemically modified biochar in soil (Model I – Keursten model, Model II – Gompertz model, Model III); Fluorescence micrographs of microbes actively degrading the extruded PHB film and PHB filled with untreated and chemically modified biochar; Alpha diversity Shannon and Simpson indexes for the bacterial communities analysed; Alpha diversity Shannon and Simpson indexes for the fungal communities analysed; SEM images and fluorescence micrographs of microbes actively degrading the extruded PHB film and PHB filled with untreated or HCl treated biochar in river sediment.

Acknowledgments

This work was supported from Operational Programme Johannes Amos Comenius OP JAC "Application potential development in the field of polymer materials in the context of circular economy compliance (POCEK)", number CZ.02.01.01/00/23_021/0009004 and the Internal Grant Agency of Tomas Bata University in Zlín, ref. no. IGA/FT/2025/008. The authors would like to thank Michal Pohořelý for providing the untreated biochar sample employed in the study.

Declaration of competing interest

The authors declare that they have no known competing financial interests or personal relationships that would influence the research reported herein.

Data availability

Data will be made available on request.

CRedit authorship contribution statement

Dagmar Šašinková: Investigation, Conceptualization, Methodology, Writing – original draft, Visualization, Formal analysis. **Markéta Julinová:** Conceptualization, Methodology, Writing – original draft, Visualization, Formal analysis, Writing – review & editing, Supervision. **Alena Kalendová:** Investigation, Writing - Review & Editing. **Martina Kaszonyiová:** Investigation. **Antonín Minařík:** Investigation. **Markéta Kadlečková:** Investigation. **Nurjahan Mahmudova:** Investigation. **Jana Šerá:** Investigation. **Marek Koutný:** Writing - Review & Editing, Funding acquisition.

References

- [1] R. Sharma, S.M. Jafari, S. Sharma, Antimicrobial bio-nanocomposites and their potential applications in food packaging, *Food Control*. 112 (2020) 107086. <https://doi.org/10.1016/j.foodcont.2020.107086>.
- [2] J.W. Rhim, H.M. Park, C.S. Ha, Bio-nanocomposites for food packaging applications, *Prog. Polym. Sci.* 38 (2013) 1629–1652. <https://doi.org/10.1016/j.progpolymsci.2013.05.008>.
- [3] H.E. Salama, G.R. Saad, M.W. Sabaa, Synthesis, characterization and antimicrobial activity of biguanidinylated chitosan-g-poly [(R)-3-hydroxybutyrate], *Int. J. Biol. Macromol.* 101 (2017) 438–447. <https://doi.org/10.1016/j.ijbiomac.2017.03.075>.

- [4] T. Ikejima, Y. Inoue, Crystallization behavior and environmental biodegradability of the blend films of poly (3-hydroxybutyric acid) with chitin and chitosan, *Carbohydr. Polym.* 41 (2000), 351–356. [https://doi.org/10.1016/S0144-8617\(99\)00105-8](https://doi.org/10.1016/S0144-8617(99)00105-8).
- [5] J.R. Xavier, S.T. Babusha, J. George, K.V. Ramana, Material properties and antimicrobial activity of polyhydroxybutyrate (PHB) films incorporated with vanillin, *Appl. Biochem. Biotechnol.* 176 (2015) 1498–1510. <https://doi.org/10.1007/s12010-015-1660-9>.
- [6] J.P. Correa, V. Molina, M. Sanchez, C. Kainz, P. Eisenberg, M.B. Massani, Improving ham shelf life with a polyhydroxybutyrate/polycaprolactone biodegradable film activated with nisin, *Food Packaging Shelf.* 11 (2017) 31–39. <https://doi.org/10.1016/j.fpsl.2016.11.004>.
- [7] C.R. Rech, K.C. da Silva Brabes, B.E.B. e Silva, P.R.S. Bittencourt, M.T. Koschevic, da T.F.S. Silveira, M.A.U. Martines, T. Caon, S.M. Martelli, Biodegradation of eugenol-loaded polyhydroxybutyrate films in different soil types, *Case Stud. Chem. Environ. Eng.* 2 (2020) 100014. <https://doi.org/10.1016/j.cscee.2020.100014>.
- [8] S.V.G. Kumari, K. Pakshirajan, G. Pugazhenthii, Development and characterization of active poly (3-hydroxybutyrate) based composites with grapeseed oil and MgO nanoparticles for shelf-life extension of white button mushrooms (*Agaricus bisporus*), *Int. J. Biol. Macromol.* 260 (2024) 129521. <https://doi.org/10.1016/j.ijbiomac.2024.129521>.
- [9] A.M. Díez-Pascual, A.L. Díez-Vicente, ZnO-reinforced poly (3-hydroxybutyrate-co-3-hydroxyvalerate) bionanocomposites with antimicrobial function for food packaging. *ACS Appl. Mater. Interfaces.* 6 (2014) 9822–9834. <https://doi.org/10.1021/am502261e>.
- [10] G.C.V. Iulianelli, G.D.S. David, T.N. dos Santos, P.J.O. Sebastião, M.I.B. Tavares, Influence of TiO₂ nanoparticle on the thermal, morphological and molecular

- characteristics of PHB matrix. *Polym. Test.* 65 (2018) 156–162.
<https://doi.org/10.1016/j.polymertesting.2017.11.018>.
- [11] P. Maiti, C.A. Batt, E.P. Giannelis, New biodegradable polyhydroxybutyrate/layered silicate nanocomposites, *Biomacromolecules*.8 (2007) 3393–3400.
<https://doi.org/10.1021/bm700500t>.
- [12] M. Hosseinnjad, S.M. Jafari, Evaluation of different factors affecting antimicrobial properties of chitosan, *Int. J. Biol. Macromol.* 85 (2016) 467–475.
<https://doi.org/10.1016/j.ijbiomac.2016.01.022>
- [13] T. Huang, Y. Qian, J. Wei, C. Zhou, Polymeric antimicrobial food packaging and its applications, *Polymers* 11 (2019) 560. <https://doi.org/10.3390/polym11030560>
- [14] S.A. Blaser, M. Scheringer, M. MacLeod, K. Hungerbühler, Estimation of cumulative aquatic exposure and risk due to silver: contribution of nano-functionalized plastics and textiles, *Sci. Total Environ.* 390 (2008) 396–409.
<https://doi.org/10.1016/j.scitotenv.2007.10.010>.
- [15] E. McGillicuddy, I. Murray, S. Kavanagh, L. Morrison, A. Fogarty, M. Cormican, P. Dockery, M. Prendergast, N. Rowan, D. Morris, Silver nanoparticles in the environment: Sources, detection and ecotoxicology, *Sci. Total Environ.* 575 (2017) 231–246,
<https://doi.org/10.1016/j.scitotenv.2016.10.041>
- [16] Z. Zhang, Q. Cui, L. Chen, X. Zhu, S. Zhao, C. Duan, X. Zhang, D. Song, L. Fang, A critical review of microplastics in the soil-plant system: Distribution, uptake, phytotoxicity and prevention, *J. Hazard. Mater.* 424 (2022) 127750.
<https://doi.org/10.1016/j.jhazmat.2021.127750>.

- [17] Y. Zheng, B. Nowack, Size-specific, dynamic, probabilistic material flow analysis of titanium dioxide releases into the environment, *Environ. Sci. Technol.* 55 (2021) 2392–2402. <https://doi.org/10.1021/acs.est.0c07446>.
- [18] H.L. Chien, Y.T. Tsai, W.S. Tseng, J.A. Wu, S.L. Kuo, S.L. Chang, S.J. Huang, C.T. Liu, Biodegradation of PBSA films by Elite *Aspergillus* Isolates and farmland soil, *Polymers* 14 (2022) 1320. <https://doi.org/10.3390/polym14071320>.
- [19] M. Julinová, D. Šašinková, A. Minařík, M. Kaszonyiová, A. Kalendová, M. Kadlečková, A. Fayyazbakhsh, M. Koutný, Comprehensive biodegradation analysis of chemically modified poly (3-hydroxybutyrate) materials with different crystal structures, *Biomacromolecules* 24 (2023) 4939–4957. <https://doi.org/10.1021/acs.biomac.3c00623>.
- [20] D.K. Mahmoud, M.A.M. Salleh, W.A.W.A. Karim, A. Idris, Z.Z. Abidin, Batch adsorption of basic dye using acid treated kenaf fibre char: Equilibrium, kinetic and thermodynamic studies, *Chem. Eng. J.* 181–182 (2012) 449–457. <https://doi.org/10.1016/j.cej.2011.11.116>.
- [21] Y. Xue, B. Gao, Y. Yao, M. Inyang, M. Zhang, A.R. Zimmerman, K.S. Ro, Hydrogen peroxide modification enhances the ability of biochar (hydrochar) produced from hydrothermal carbonization of peanut hull to remove aqueous heavy metals: Batch and column tests, *Chem. Eng. J.* 200–202 (2012) 673–680. <https://doi.org/10.1016/j.cej.2012.06.116>.
- [22] M.D. Huff, J.W. Lee, Biochar-surface oxygenation with hydrogen peroxide. *J. Environ. Manage.* 165 (2016) 17–21. <https://doi.org/10.1016/j.jenvman.2015.08.046>.
- [23] M. Julinová, L. Vaňharová, M. Jurča, A. Minařík, P. Duchek, J. Kavečková, D. Rouchalová, P. Skácelík, Effect of different fillers on the biodegradation rate of thermoplastic starch in

- water and soil environments, *J. Polym. Environ.* 28 (2020) 566–583.
<https://doi.org/10.1007/s10924-019-01624-7>
- [24] M.M. Quispe, O.V. Lopez, D.A. Boina, J. F. Stumbé, M.A. Villar, Glycerol-based additives of poly (3-hydroxybutyrate) films. *Polym. Test.* 93 (2021) 107005.
<https://doi.org/10.1016/j.polymertesting.2020.107005>.
- [25] J. Šerá, L. Serbruyns, B. De Wilde, M. Koutný, Accelerated biodegradation testing of slowly degradable polyesters in soil, *Polym. Degrad. Stab.* 171 (2020) 109031,
<https://doi.org/10.1016/j.polymdegradstab.2019.109031>.
- [26] International Organization for Standardization. (2019). ISO 17556: Plastics — Determination of the ultimate aerobic biodegradability of plastic materials in soil by measuring the oxygen demand in a respirometer or the amount of carbon dioxide evolved. Geneva, Switzerland: ISO.
- [27] G.T. Keursten, P.H. Groenevelt, Biodegradation of rubber particles in soil, *Biodegradation* 7 (1996) 329–333. <https://doi.org/10.1007/BF00115746>.
- [28] S. Kwon, M.C. Zambrano, R.A. Venditti, J.J. Pawlak, Aerobic aquatic biodegradation of bio-based and biodegradable polymers: Kinetic modeling and key factors for biodegradability, *Int. Biodeterior. Biodegrad.* 185 (2023) 105671.
<https://doi.org/10.1016/j.ibiod.2023.105671>.
- [29] D. Rial, J.A. Vázquez, M.A. Murado, Effects of three heavy metals on the bacteria growth kinetics: a bivariate model for toxicological assessment, *Appl. Microbiol. Biotechnol.* 90 (2011) 1095–1109. <https://doi.org/10.1007/s00253-011-3138-1>.
- [30] E.M. White, J. Horn, S. Wang, B. Crawford, B.W. Ritchie, D. Carraway, J. Locklin, Comparative study of the biological degradation of poly (3-hydroxybutyrate-co-3-

- hydroxyhexanoate) microbeads in municipal wastewater in environmental and controlled laboratory conditions, *Environ. Sci. Technol.* 55 (2021) 11646–11656. <https://doi.org/10.1021/acs.est.1c00974>.
- [31] Czech Standards Institute. (2017). ČSN 75 7221: Water quality – Classification of surface water quality. Prague: Czech Standards Institute.
- [32] International Organization for Standardization. (2016). ISO 19679: Plastics — Determination of aerobic biodegradation of non-floating plastic materials in a seawater/sediment interface — Method by analysis of evolved carbon dioxide. Geneva, Switzerland: ISO.
- [33] Illumina. 16S Metagenomic sequencing library preparation: Preparing 16S ribosomal RNA gene amplicons for the illumina MiSeq system; Illumina, 2013.
- [34] B.J. Callahan, P.J. McMurdie, M.J. Rosen, A.W. Han, A.J.A. Johnson, S.P. Holmes, DADA2: High-resolution sample inference from Illumina amplicon data, *Nat. Methods* 13 (2016) 581–583. <https://doi.org/10.1038/nmeth.3869>.
- [35] C. Quast, E. Pruesse, P. Yilmaz, J. Gerken, T. Schweer, P. Yarza, J. Peplies, F.O. Glöckner, The SILVA ribosomal RNA gene database project: improved data processing and web-based tools, *Nucleic Acids Res.* 41 (2012) D590–D596. <https://doi.org/10.1093/nar/gks1219>.
- [36] U. Kõljalg, H.R. Nilsson, D. Schigel, L. Tedersoo, K.H. Larsson, T.W. May, A.F.S. Taylor, T.S. Jeppesen, T.G. Frøslev, B.D. Lindahl, K. Põldmaa, I. Saar, A. Suija, A. Savchenko, I. Yatsiuk, K. Adojaan, F. Ivanov, T. Piirmann, R. Pöhönen, A. Zirk, K. Abarenkov, The taxon hypothesis paradigm—on the unambiguous detection and communication of taxa, *Microorganisms* 8 (2020) 1910. <https://doi.org/10.3390/microorganisms8121910>.

- [37] P.J. McMurdie, S. Holmes, Phyloseq: an R package for reproducible interactive analysis and graphics of microbiome census data, *PLoS One* 8 (2013) e61217. <https://doi.org/10.1371/journal.pone.0061217>.
- [38] C. Liu, Y. Cui, X. Li, M. Yao, Microeco: an R package for data mining in microbial community ecology, *FEMS Microbiol. Ecol.* 97 (2021) fiae255. <https://doi.org/10.1093/femsec/fiae255>.
- [39] I. Szymanek, M. Cvek, D. Rogacz, A. Żarski, K. Lewicka, V. Sedlarik, P. Rychter, Degradation of polylactic acid/polypropylene carbonate films in soil and phosphate buffer and their potential usefulness in agriculture and agrochemistry, *Int. J. Mol. Sci.* 25 (2024) 653. <https://doi.org/10.3390/ijms25010653>.
- [40] C. Kopp, P. Sica, C. Lu, D. Tobler, L.S. Jensen, D. Müller-Stöver, Increasing phosphorus plant availability from P-rich ashes and biochars by acidification with sulfuric acid, *J. Environ. Chem. Eng.* 11 (2023) 111489. <https://doi.org/10.1016/j.jece.2023.111489>.
- [41] L.C. Almeida, A.S. Barbosa, A.T. Fricks, L.S. Freitas, Á.S. Lima, C.M. Soares, Use of conventional or non-conventional treatments of biochar for lipase immobilization, *Process Biochem.* 61 (2017) 124–129. <https://doi.org/10.1016/j.procbio.2017.06.020>.
- [42] Y. Zhang, Y. Zheng, Y. Yang, J. Huang, A.R. Zimmerman, H. Chen, X. Hu, B. Gao, Mechanisms and adsorption capacities of hydrogen peroxide modified ball milled biochar for the removal of methylene blue from aqueous solutions, *Bioresour. Technol.* 337 (2021) 125432. <https://doi.org/10.1016/j.biortech.2021.125432>.
- [43] Z. Wang, J. Li, G. Zhang, Y. Zhi, D. Yang, X. Lai, T. Ren, Characterization of acid-aged biochar and its ammonium adsorption in an aqueous solution, *Materials* 13 (2020) 2270. <https://doi.org/10.3390/ma13102270>.

- [44] R. Muvhiiwa, A. Kuvarega, E.M. Llana, A. Muleja, Study of biochar from pyrolysis and gasification of wood pellets in a nitrogen plasma reactor for design of biomass processes, *J. Environ. Chem. Eng.* 7 (2019) 103391. <https://doi.org/10.1016/j.jece.2019.103391>.
- [45] A. Silber, I. Levkovitch, E.R. Graber, pH-dependent mineral release and surface properties of cornstraw biochar: agronomic implications, *Environ. Sci. Technol.* 44 (2010) 9318–9323. <https://doi.org/10.1021/es101283d>.
- [46] C. Zhou, X. Song, Y. Wang, H. Wang, S. Ge, The sorption and short-term immobilization of lead and cadmium by nano-hydroxyapatite/biochar in aqueous solution and soil, *Chemosphere* 286 (2022) 131810. <https://doi.org/10.1016/j.chemosphere.2021.131810>.
- [47] L. Trakal, D. Bingöl, M. Pohořelý, M. Hruška, M. Komárek, Geochemical and spectroscopic investigations of Cd and Pb sorption mechanisms on contrasting biochars: engineering implications, *Bioresour. Technol.* 171 (2014) 442–451. <https://doi.org/10.1016/j.biortech.2014.08.108>.
- [48] B. Li, J. Guo, K. Lv, J. Fan, Adsorption of methylene blue and Cd (II) onto maleylated modified hydrochar from water, *Environ. Pollut.* 254 (2019) 113014. <https://doi.org/10.1016/j.envpol.2019.113014>.
- [49] G. Zhang, D. Wu, W. Xie, Z. Wang, C. Xu, Green poly (β -hydroxybutyrate)/starch nanocrystal composites: tuning the nucleation and spherulite morphology through surface acetylation of starch nanocrystal, *Carbohydr. Polym.* 195 (2018) 79–88. <https://doi.org/10.1016/j.carbpol.2018.04.079>.
- [50] X. Zhou, T.B. Moghaddam, M. Chen, S. Wu, S. Adhikari, Biochar removes volatile organic compounds generated from asphalt, *Sci. Total Environ.* 745 (2020) 141096. <https://doi.org/10.1016/j.scitotenv.2020.141096>.

- [51] X. Jia, R. Peng, H. Huang, J. Dan, M. Lu, D. Zhang, J. Wang, D. Li, H. Fang, C. Yu, Lotus leaves-derived MnO_x/biochar as an efficient catalyst for low-temperature NH₃-SCR removal of NO_x: effects of modification methods of biochar, *J. Chem. Technol. Biotechnol.* 97 (2022) 3100–3110. <https://doi.org/10.1002/jctb.7175>.
- [52] A. Pustak, I. Pucić, M. Denac, I. Švab, J. Pohleven, V. Musil, I. Šmit, Morphology of polypropylene/silica nano- and microcomposites, *J. Appl. Polym. Sci.* 128 (2013) 3099–3106. <https://doi.org/10.1002/app.38487>.
- [53] A.A. Alghyamah, A.Y. Elnour, H. Shaikh, S. Haider, A.M. Poulouse, S.M. Al-Zahrani, W.A. Almasry, S.Y. Park, Biochar/polypropylene composites: A study on the effect of pyrolysis temperature on crystallization kinetics, crystalline structure, and thermal stability, *J. King Saud Univ. Sci.* 33 (2021) 101409. <https://doi.org/10.1016/j.jksus.2021.101409>.
- [54] K. Wang, J. Wu, H. Zeng, Radial growth rate of spherulites in polypropylene/barium sulfate composites, *Eur. Polym. J.* 39 (2003) 1647–1652. [https://doi.org/10.1016/S0014-3057\(03\)00071-5](https://doi.org/10.1016/S0014-3057(03)00071-5).
- [55] Y. Zhou, D. Li, X. Li, Y. Li, B. Li, F. Zhou, A comparison of chitosan adhesion to KOH and H₂O₂ pre-treated electrospun poly (3-hydroxybutyrate) nanofibers, *Fibers* 11 (2023) 91. <https://doi.org/10.3390/fib11110091>.
- [56] C.A. Woolnough, T. Charlton, L.H. Yee, M. Sarris, L.J.R. Foster, Surface changes in polyhydroxyalkanoate films during biodegradation and biofouling, *Polym. Int.* 57 (2008) 1042–1051. <https://doi.org/10.1002/pi.2444>.
- [57] P.P. Kundu, J. Biswas, H. Kim, S. Choe, Influence of film preparation procedures on the crystallinity, morphology and mechanical properties of LLDPE films, *Eur. Polym. J.* 39 (2003) 1585–1593. [https://doi.org/10.1016/S0014-3057\(03\)00056-9](https://doi.org/10.1016/S0014-3057(03)00056-9).

- [58] M. Aflori, Embedding silver nanoparticles at PHB surfaces by means of combined plasma and chemical treatments, *Rev. Roum. Chim.* 61 (2016) 405–409.
- [59] J.R. Banu, M. Gunasekaran, Augmentation in polyhydroxybutyrate and biogas production from waste activated sludge through mild sonication induced thermo-fenton disintegration, *Bioresour. Technol.* 369 (2023) 128376. <https://doi.org/10.1016/j.biortech.2022.128376>.
- [60] K. Csomorova, J. Rychlý, D. Bakoš, I. Janigova, The effect of inorganic additives on the decomposition of poly (beta-hydroxybutyrate) into volatile products, *Polym. Degrad. Stab.* 43 (1994) 441–446. [https://doi.org/10.1016/0141-3910\(94\)90017-5](https://doi.org/10.1016/0141-3910(94)90017-5).
- [61] P. Maiti, C. Batt, Renewable plastics: synthesis and properties of PHB nanocomposites, *Polym. Mater. Sci. Engng.* 88 (2003) 58–59.
- [62] J. Yu, D. Plackett, L.X. Chen, Kinetics and mechanism of the monomeric products from abiotic hydrolysis of poly [(R)-3-hydroxybutyrate] under acidic and alkaline conditions, *Polym. Degrad. Stab.* 89 (2005) 289–299. <https://doi.org/10.1016/j.polymdegradstab.2004.12.026>.
- [63] T. Haeldermans, P. Samyn, R. Cardinaels, D. Vandamme, K. Vanreppelen, A. Cuypers, S. Schreurs, Bio-based poly(3-hydroxybutyrate)/thermoplastic starch composites as a host matrix for biochar fillers, *J. Polym. Environ.* 29 (2021) 2478–2491. <https://doi.org/10.1007/s10924-021-02049-x>.
- [64] S.G. Hong, Y.C. Lin, C.H. Lin, Improvement of the thermal stability of polyhydroxybutyrates by grafting with maleic anhydride by different methods: differential scanning calorimetry, thermogravimetric analysis and gel permeation chromatography, *J. Appl. Polym. Sci.* 110 (2008) 2718–2726. <https://doi.org/10.1002/app.28782>.

- [65] S. Nizamuddin, A. Jadhav, S.S. Qureshi, H.A. Baloch, M.T.H. Siddiqui, N.M. Mubarak, G. Griffin, S. Madapusi, A. Tanksale, M.I. Ahamed, Synthesis and characterization of polylactide/rice husk hydrochar composite, *Sci. Rep.* 9 (2019) 1–11. <https://doi.org/10.1038/s41598-019-41960-1>.
- [66] C. Wang, C.H. Hsu, I.H. Hwang, Scaling laws and internal structure for characterizing electrospun poly [(R)-3-hydroxybutyrate] fibers, *Polymer* 49 (2008) 4188–4195. <https://doi.org/10.1016/j.polymer.2008.07.033>.
- [67] M. Mohammadalipour, M. Asadolahi, Z. Mohammadalipour, T. Behzad, S. Karbasi, Plasma surface modification of electrospun polyhydroxybutyrate (PHB) nanofibers to investigate their performance in bone tissue engineering, *Int. J. Biol. Macromol.* 230 (2023) 123167. <https://doi.org/10.1016/j.ijbiomac.2023.123167>.
- [68] S. Dhaniala, M. Bernela, R. Rani, M. Parsad, R. Kumar, R. Thakur, Polyhydroxybutyrate (PHB) in nanoparticulate form improves physical and biological performance of scaffolds, *Int. J. Biol. Macromol.* 236 (2023) 123875. <https://doi.org/10.1016/j.ijbiomac.2023.123875>.
- [69] S. Holešová, K. Čech Barabaszová, M. Hundáková, M. Ščuková, K. Hrabovská, K. Jozzko, M. Antonowicz, B.D. Gzik-Zroska, Development of novel thin polycaprolactone (PCL)/clay nanocomposite films with antimicrobial activity promoted by the study of mechanical, thermal, and surface properties, *Polymers* 13 (2021) 3193. <https://doi.org/10.3390/polym13183193>.
- [70] B. Laycock, M. Nikolić, J.M. Colwell, E. Gauthier, P. Halley, S. Bottle, G. George, Lifetime prediction of biodegradable polymers, *Prog. Polym. Sci.* 71 (2017) 144–189. <https://doi.org/10.1016/j.progpolymsci.2017.02.004>.

- [71] D. Merino, A. Athanassiou, Biodegradable and active mulch films: Hydrolyzed lemon peel waste and low methoxyl pectin blends with incorporated biochar and neem essential oil, *ACS Sustain. Chem. Eng.* 10 (2022) 10789–10802. <https://doi.org/10.1021/acssuschemeng.2c01539>.
- [72] D. She, J. Dong, J. Zhang, L. Liu, Q. Sun, Z. Geng, P. Peng, Development of black and biodegradable biochar/gutta percha composite films with high stretchability and barrier properties, *Compos. Sci. Technol.* 175 (2019) 1–5. <https://doi.org/10.1016/j.compscitech.2019.03.007>.
- [73] Y. Yu, H. Guo, Z. Zhong, Z. Lu, Z. Li, Z. Chang, Enhanced removal of tetrabromobisphenol A by *Burkholderia cepacia* Y17 immobilized on biochar, *Ecotox. Environ. Safe.* 249 (2023) 114450. <https://doi.org/10.1016/j.ecoenv.2022.114450>.
- [74] C. Wu, D. Zhi, B. Yao, Y. Zhou, Y. Yang, Y. Zhou, Immobilization of microbes on biochar for water and soil remediation: A review, *Environ. Res.* 212 (2022) 113226. <https://doi.org/10.1016/j.envres.2022.113226>.
- [75] P. Pitter, J. Chudoba, *Biodegradability of Organic Substance in the Aquatic Environment*, 1990, ISBN 08-493-51316.
- [76] T.F. Nelson, R. Baumgartner, M. Jaggi, S.M. Bernasconi, G. Battagliarin, C. Sinkel, A. Kunkel, H.-P.E. Kohler, K. McNeill, M. Sander, Biodegradation of poly(butylene succinate) in soil laboratory incubations assessed by stable carbon isotope labelling, *Nat. Commun.* 13 (2022) 5691. <https://doi.org/10.1038/s41467-022-33064-8>.
- [77] A. Calmon, F. Silvestre, V. Bellon-Maurel, J.M. Roger, P. Feuilloley, Modelling easily biodegradability of materials in liquid medium – relationship between structure and

- biodegradability, J. Environ. Polym. Degrad. 7 (1999) 135–144. <https://doi.org/10.1023/A:1022845605474>.
- [78] A.M. Gibson, N. Bratchell, T.A. Roberts, The effect of sodium chloride and temperature on the rate and extent of growth of *Clostridium botulinum* type A in pasteurized pork slurry, J. Appl. Microbiol. 62 (1987) 479–490. <https://doi.org/10.1111/j.1365-2672.1987.tb02680.x>.
- [79] H. Nishida, Y. Tokiwa, Effects of higher-order structure of poly(3-hydroxybutyrate) on its biodegradation. II. Effects of crystal structure on microbial degradation, J. Environ. Polym. Degr. 1 (1993) 65–80. <https://doi.org/10.1007/BF0145765>.
- [80] H. Tsuji, K. Suzuyoshi, Environmental degradation of biodegradable polyesters 1. Poly (ϵ -caprolactone), poly [(R)-3-hydroxybutyrate], and poly (L-lactide) films in controlled static seawater, Polym. Degrad. Stab. 75 (2002) 347–355. [https://doi.org/10.1016/S0141-3910\(01\)00240-3](https://doi.org/10.1016/S0141-3910(01)00240-3).
- [81] K. Numata, H. Abe, T. Iwata, Biodegradability of poly(hydroxyalkanoate) materials, Materials 2 (2009) 1104–1126. <https://doi.org/10.3390/ma2031104>.
- [82] E. Akdoğan, H.T. Şirin, G. Şahal, Z. Deniz, A. Kaya, D.Ç. Serdaroğlu, Accelerating the environmental biodegradation of poly-3-hydroxybutyrate (PHB) via plasma surface treatment, Bioresour. Technol. Rep. 25 (2024) 101719. <https://doi.org/10.1016/j.biteb.2023.101719>.
- [83] D.G. Goodwin, Z. Xia, T.B. Gordon, C. Gao, E.J. Bouwer, D.H. Fairbrother, Biofilm development on carbon nanotube/polymer nanocomposites, Environ. Sci.: Nano 3 (2016) 545–558. <https://doi.org/10.1039/C5EN00277J>.

- [84] S. Dey, P. Tribedi, Microbial functional diversity plays an important role in the degradation of polyhydroxybutyrate (PHB) in soil, *3 Biotech* 8 (2018). <https://doi.org/10.1007/s13205-018-1201-7>.
- [85] M. Bassas-Galià, B. Nogales, S. Arias, M. Rohde, K.N. Timmis, G. Molinari, Plant original *Massilia* isolates producing polyhydroxybutyrate, including one exhibiting high yields from glycerol, *J. Appl. Microbiol.* 112 (2012) 443–454. <https://doi.org/10.1111/j.1365-2672.2011.05228.x>.
- [86] H. Xu, X. Wang, H. Li, H. Yao, J. Su, Y. Zhu, Biochar impacts soil microbial community composition and nitrogen cycling in an acidic soil planted with rape, *Environ. Sci. Technol.* 48 (2014) 9391–9399. <https://doi.org/10.1021/es5021058>.
- [87] G. Choppala, N. Bolan, M. Megharaj, Z. Chen, R. Naidu, The influence of biochar and black carbon on reduction and bioavailability of chromate in soils, *J. Environ. Qual.* 41 (2012) 1175–1184. <https://doi.org/10.2134/jeq2011.0145>.
- [88] A.U. Osadebe, P.U. Patrick, Environmental detoxification potential of axenic and mixed cultures of *Bacillus* species on pesticides using an in vitro biodegradation assay, *J. Microbiol. Biotechnol. Food Sci.* (2023) e9272. <https://doi.org/10.55251/jmbfs.9272>.
- [89] A.B. Mesquita, I.V. Silva, C.J.F. Braz, L.H. Carvalho, R. Barbosa, J.H.L.F. Paranagua, T.S. Alves, Characterization of PHB/clay biocomposites exposed to degradation in an aquatic environment, *Mater. Res.* 26 (2023). <https://doi.org/10.1590/1980-5373-mr-2023-015>.
- [90] N. Altaee, G.A. El-Hiti, A. Fahdil, K. Sudesh, E. Yousif, Biodegradation of different formulations of polyhydroxybutyrate films in soil, *SpringerPlus* 5 (2016). <https://doi.org/10.1186/s40064-016-2480-2>.

- [91] S. Lee, L. Ten, K. Das, Y. You, H. Jung, Biodegradative activities of fungal strains isolated from terrestrial environments in Korea, *Mycobiology* (2021) 1–9. <https://doi.org/10.1080/12298093.2021.1903131>.
- [92] B. Xi, B. Wang, M. Chen, X. Lee, X. Zhang, S. Wang, Z. Yu, P. Wu, Environmental behaviors and degradation methods of microplastics in different environmental media, *Chemosphere* 299 (2022) 134354. <https://doi.org/10.1016/j.chemosphere.2022.134354>.
- [93] S. Wang, C. Song, W. Mizuno, M. Sano, M. Maki, Ch. Yang, B. Zhang, S. Takeuchi, Estimation on biodegradability of poly(3-hydroxybutyrate-co-3-hydroxyvalerate) (PHB/V) and numbers of aerobic PHB/V degrading microorganisms in different natural environments, *J. Polym. Environ.* 13 (2005) 39–45. <https://doi.org/10.1007/s10924-004-1214-7>.
- [94] T.G. Volova, M.I. Gladyshev, M.Y. Trusova, N.O. Zhila, Degradation of polyhydroxyalkanoates in eutrophic reservoir, *Polym. Degrad. Stab.* 92 (2007) 580–586. <https://doi.org/10.1016/j.polymdegradstab.2007.01.011>.
- [95] R. Kadoya, N. Tanaka, N. Fujita, Y. Shiwa, S. Taguchi, Changed bacterial community in the river water samples upon introduction of biodegradable poly(3-hydroxybutyrate), *Polym. Degrad. Stab.* 176 (2020) 109144. <https://doi.org/10.1016/j.polymdegradstab.2020.109144>.
- [96] E. Syranidou, K. Karkanorachaki, F. Amorotti, M. Franchini, E. Repouskou, M. Kaliva, M. Vamvakaki, B. Kolvenbach, F. Fava, P.F.-X. Corvini, N. Kalogerakis, Biodegradation of weathered polystyrene films in seawater microcosms, *Sci. Rep.* 7 (2017) 1–12. <https://doi.org/10.1038/s41598-017-18366-y>.

- [97] I.L. Smith, T. Stanton, A. Law, Plastic habitats: Algal biofilms on photic and aphotic plastics, *J. Hazard. Mater. Lett.* 2 (2021) 100038. <https://doi.org/10.1016/j.hazl.2021.100038>.
- [98] A. Nauendorf, S. Krause, N.K. Bigalke, E.V. Gorb, S.N. Gorb, M. Haeckel, M. Wahl, T. Treude, Microbial colonization and degradation of polyethylene and biodegradable plastic bags in temperate fine-grained organic-rich marine sediments, *Mar. Pollut. Bull.* 103 (2016) 168–178. <https://doi.org/10.1016/j.marpolbul.2015.12.024>.
- [99] S. van Grinsven, C. Schubert, Soil-biodegradable plastic films do not decompose in a lake sediment over 9 months of incubation, *Biogeosciences* 20 (2023) 4213–4220. <https://doi.org/10.5194/bg-20-4213-2023>.
- [100] E. Liwarska-Bizukojc, Phytotoxicity assessment of biodegradable and non-biodegradable plastics using seed germination and early growth tests, *Chemosphere* 289 (2022) 133132. <https://doi.org/10.1016/j.chemosphere.2021.133132>.
- [101] E. Balestri, V. Menicagli, V. Ligorini, S. Fulignati, A.M.R. Galletti, C. Lardicci, Phytotoxicity assessment of conventional and biodegradable plastic bags using seed germination test, *Ecol. Indic.* 102 (2019) 569–580. <https://doi.org/10.1016/j.ecolind.2019.03.005>.
- [102] A. McCauley, C. Jones, J. Jacobsen, Soil pH and organic matter, *Nutrient Management Module 8* (2009) 1–12.
- [103] R Core Team, *R: A Language and Environment for Statistical Computing*, R Foundation for Statistical Computing, Vienna, Austria, 2013.

List of Tables

Table 1 Basic characterization of the extruded PHB and PHB-biochar films (n=10, average \pm standard deviation)

Table 2 Data for characterization from DSC thermograms (a second heating scan) on the extruded PHB film and specimens with untreated or chemically modified biochar (degree of crystallinity – X_c ; melting temperature – T_m for the chemically modified phase; crystallization temperature – T_c ; average \pm standard deviation, n=3)

Table 3 Data from TGA analysis on the extruded PHB film and PHB filled with the untreated or chemically modified biochar

Table 4 TGA analysis - percentage changes of monitored characteristics of PHB filled with untreated and chemically modified biochars compared to the reference (extruded PHB)

Table 5 Comparison of experimental (absolute) results and prediction of biodegradation by kinetic modelling with statistical indicators (R-correlation coefficient, R^2 -determination

coefficient) for the approximation of CO₂ kinetic curves by Models I, II and III with (+/-) signs denoting relevance (average ± standard deviation, n=3)

Table 6 Qualitative analysis of the microstructures of the extruded PHB film and specimens filled with untreated or chemically modified biochar, as per their degradation within 150 days [81,82]

Table 1

SAMPLE NAME	TC* (%)	thickness (µm)	leaching experiments** (pH)		water uptake in equilibrium (%)
			24 h	168 h	
extruded PHB	55.93 ± 0.02	204 ± 0.012	6.26	6.12	0.11 ± 0.31
BC	55.58 ± 0.05	233 ± 0.038	6.05	5.83	0.25 ± 0.19
BC-HCl	55.64 ± 0.07	151 ± 0.030	6.14	6.13	0.13 ± 0.11
BC-MA	55.78 ± 0.14	167 ± 0.014	5.98	6.01	0.17 ± 0.10
BC-H ₂ O ₂	55.72 ± 0.02	151 ± 0.012	5.76	5.82	0.29 ± 0.20

* TC – total carbon (Automatic Elementar Analyzer, Thermos Fisher Scientific Inc.)

** pH of the aqueous leachate of the films, as determined after 24 h and 168 h (0.1 g of the tested film and 25 ml H₂O)

Table 2

Sample	T_m °C	X_c %	T_c °C
extruded PHB	168.72	57.05	86.53
BC	169.55	57.79	92.05
BC-HCl	169.74	63.18	94.41
BC-MA	169.80	63.16	93.24
BC-H ₂ O ₂	168.89	57.78	90.36

Table 3

Sample	T_{onset1}	T_{max1}	Δm1	m_{residual1}	m_{residual}
	°C	°C	%	%	total
					%
extruded PHB (ref.)	282	295	99.58	1.46	1.19
BC	280	297	98.98	1.25	1.06
BC-HCl	279	295	99.06	1.69	1.49
BC-MA	282	297	98.9	1.94	1.51
BC-H ₂ O ₂	280	294	98.32	2.46	2.13

Table 4

Sample	T_{onset1} °C	T_{max1} °C	Δm1 %	m_{residual1} %	m_{residual} total %
extruded PHB (ref.)	100.00	100.00	100.00	100.00	100.00
BC	0.71	-0.68	0.60	14.38	10.92
BC-HCl	1.06	0.00	0.52	-15.75	-25.21
BC-MA	0.00	-0.68	0.68	-32.88	-26.89
BC-H ₂ O ₂	0.71	0.34	1.27	-68.49	-78.99

Table 5

	D_{max} %	k_{MAX} days ⁻¹	t_{lag} days	R²	R	signs (+/-)
Cellulose						
absolute	88.45 ± 10.83	-	5.2 ± 0.6	-	-	
M I	86.38 ± 1.47	23.9 ± 1.48 × 10 ⁻³	1.83 ± 0.96	0.9873	0.9936	+
M II	82.17 ± 1.80	1.289 ± 0.123	-1.22 ± 3.14**	0.9665	0.9831	-
M III	-	-	-	-	-	NA
PHB						
absolute	86.52 ± 14.59	-	17.0 ± 7.21	-	-	
M I*	212.9 ± 44.7	2.90 ± 0.76 × 10 ⁻³	22.51 ± 2.19	0.9912	0.9956	-
M II	96.88 ± 2.33	0.617 ± 0.015	31.29 ± 1.51	0.9969	0.9984	-
M III	98.58 ± 2.78	0.618 ± 0.018	20.62 ± 3.86	0.9970	0.9985	+
BC						
absolute	64.39 ± 12.98	-	14.33 ± 6.37	-	-	
M I*	95.55 ± 8.11	6.30 ± 0.86 × 10 ⁻³	23.31 ± 1.84	0.9901	0.9950	-
M II	67.07 ± 0.93	0.529 ± 0.011	28.39 ± 1.13	0.9982	0.9991	-
M III	69.35 ± 1.41	0.521 ± 0.014	19.79 ± 3.07	0.9974	0.9987	+
BC-HCl						
absolute	37.02 ± 8.17	-	25.00 ± 6.54	-	-	
M I*	48.89 ± 2.38	7.85 ± 0.68 × 10 ⁻³	28.03 ± 1.27	0.9949	0.9974	-
M II	37.22 ± 0.82	0.316 ± 0.011	30.89 ± 1.87	0.9950	0.9975	+
M III	38.50 ± 1.36	0.306 ± 0.016	23.07 ± 5.22	0.9914	0.9957	+
BC-MA						
absolute	71.63 ± 7.67	-	16.00 ± 2.59	-	-	
M I*	107.7 ± 10.98	6.2 ± 1.01 × 10 ⁻³	24.89 ± 2.09	0.9865	0.9932	-

M II	73.97 ± 0.89	0.612 ± 0.011	31.61 ± 0.99	0.9986	0.9993	-
M III	74.95 ± 1.42	0.611 ± 0.018	26.44 ± 2.73	0.9972	0.9986	+
BC-H₂O₂						
absolute	55.90 ± 0.63	-	14.83 ± 5.35	-	-	
M I*	72.40 ± 3.31	8.18 ± 0.69 × 10 ⁻³	20.19 ± 1.36	0.9942	0.9971	-
M II	57.46 ± 1.37	0.463 ± 0.018	21.38 ± 2.10	0.9936	0.9968	+
M III	63.86 ± 2.58	0.435 ± 0.018	2.34 ± 6.69	0.9936	0.9968	-

* After the correction of the lag phase.

** Negative lag phase parameter suggesting rapid mineralization of the cellulose by microbial catabolism on day 0 [30].

NA – Not Applicable, indicates models whose solution did not fit the experimental data.

Table 6

extruded PHB (ref.)	
0	Intact surface and dirt particles (Fig. S5)
10	Surface colonization, bacteria and extended structures, such as fungal filaments
30	Crystalline phase in the form of large spherulites; intensive bacterial colonization
90	Cavities; formation of an exopolysaccharide matrix [82]
150	Disordered, chain-packing crystalline regions; some crystalline lamellae [81]; cavities
BC	
0	Intact surface; random distribution of biochar particles and dirt particles (Fig. S5)
10	Relatively intact surface with only a few small cracks; some fungal filaments, typical of fungal growth
30	Degradation of the surface amorphous phase; an individual colony of bacteria, with biochar particles colonized by bacteria [73,74]
90	Crystalline phase with large spherulites; the nucleation of PHB crystals by environmental processes [19,80]; an individual colony of bacteria, with biochar particles colonized by bacteria (Fig. 11) [74]
150	Disordered, chain-packing crystalline regions; destruction of spherocrystals, with unclear contours; formation of an exopolysaccharide matrix
BC-HCl	
0	Intact surface; random distribution of biochar particles and dirt particles (Fig. S5)
10	Intensive surface colonization by bacteria, spores and extended structures, such as fungal filaments; biodegradation of the surface amorphous layer
30	Biodegradation of the surface amorphous layer; spores and fungal filaments bound to the surface (Fig. 11)
90	Crystalline phase
150	Disordered, chain-packing crystalline regions; crystals possessed molecules produced during degradation
BC-MA	
0	Numerous cracks; random distribution of biochar particles and dirt particles (Fig. S5)

10	Biofilm formation; a long fracture with pores and cracks
30	Crystalline phase with large evident spherulites; the nucleation of PHB crystals by environmental processes [19,80]; formation of an exopolysaccharide matrix
90	Crystalline phase with spherulites and disordered, chain-packing crystalline regions
150	Crystalline phase with disordered, chain-packing crystalline regions; crystals possessed molecules produced during degradation
<hr/>	
BC-H ₂ O ₂	
0	Intact surface; agglomerates of biochar particles and dirt particles (Fig. S5)
10	Relatively smooth and intact surface
30	Biofilm formation; a long fracture with pores
90	Crystalline phase with large spherulites; the lamellae of spherulites in relief
150	Crystalline phase with large spherulites; the lamellae of the spherulites in relief; no spherical degradation pattern
<hr/>	

List of Figures

- Figure 1. FTIR spectra for the non-treated and chemically modified biochars, across the range of 1850 – 600 cm⁻¹.
- Figure 2. XRD diffractograms for the untreated and chemically modified biochars.
- Figure 3. Polarized optical micrographs of the extruded PHB film and PHB filled with untreated or chemically modified biochar (at 10x magnification).
- Figure 4. Surface nano texture (colour images) and phase contrast (phase images) of the extruded PHB film and PHB filled with the untreated or chemically modified biochar, as characterized by AFM; the small black-and-white pictures are previews of threshold phase images.
- Figure 5. FTIR spectrum for the extruded PHB film and PHB filled with untreated or chemically modified biochar; left: 1850 – 500 cm⁻¹; right: 2800 – 3050 cm⁻¹.
- Figure 6. XRD diffractograms for the extruded PHB film and PHB filled with untreated or chemically modified biochar.

- Figure 7. TG curves (a) and DTG (b) curves for the extruded PHB film and PHB filled with untreated or chemically modified biochar.
- Figure 8. Surface wettability of the extruded PHB film and PHB filled with untreated or chemically modified biochar (average \pm standard deviation, n=3).
- Figure 9. Biodegradation in soil of the extruded PHB film and PHB filled with untreated or chemically modified biochar (55% soil humidity, 25°C).
- Figure 10. SEM images depicting the biodegradation of the extruded PHB film and PHB with untreated or chemically modified biochar; 55% soil humidity, 25°C; (10 days – magnification 3000x; 30, 90 and 150 days – magnification 5000x).
- Figure 11. SEM images (magnification: BC 3000 \times , BC-MA 1000 \times) and fluorescence micrographs (magnification 20 \times) of microbes actively degrading the PHB film (green = live, red = dead) in the soil environment (55% humidity, 25°C).
- Figure 12. Composition of bacterial (left) and fungal (right) communities on the surfaces of the investigated materials after 14 and 21 days of incubation in soil; sampling of background soil communities at 0, 14 and 21 days for control purposes is also detailed.
- Figure 13. Biodegradation of the extruded PHB film and PHB filled with untreated or chemically modified biochar in river sediment.

Fig. 1.

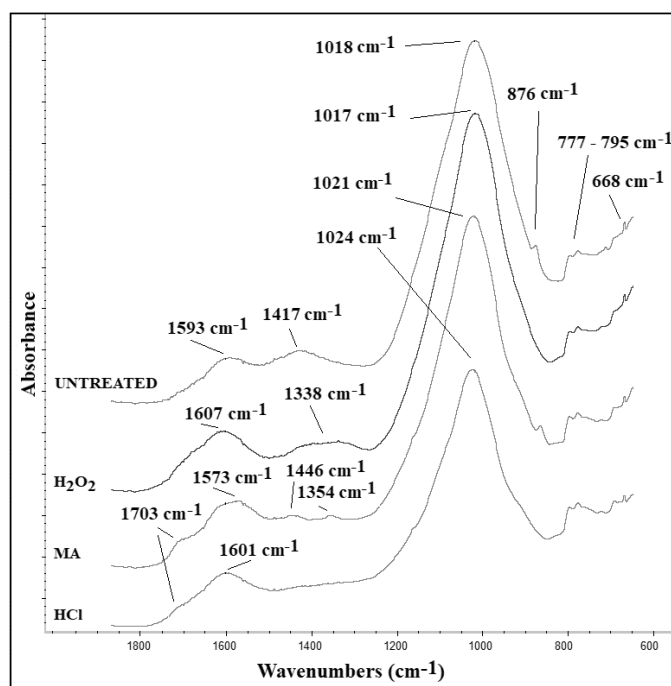


Fig. 2.

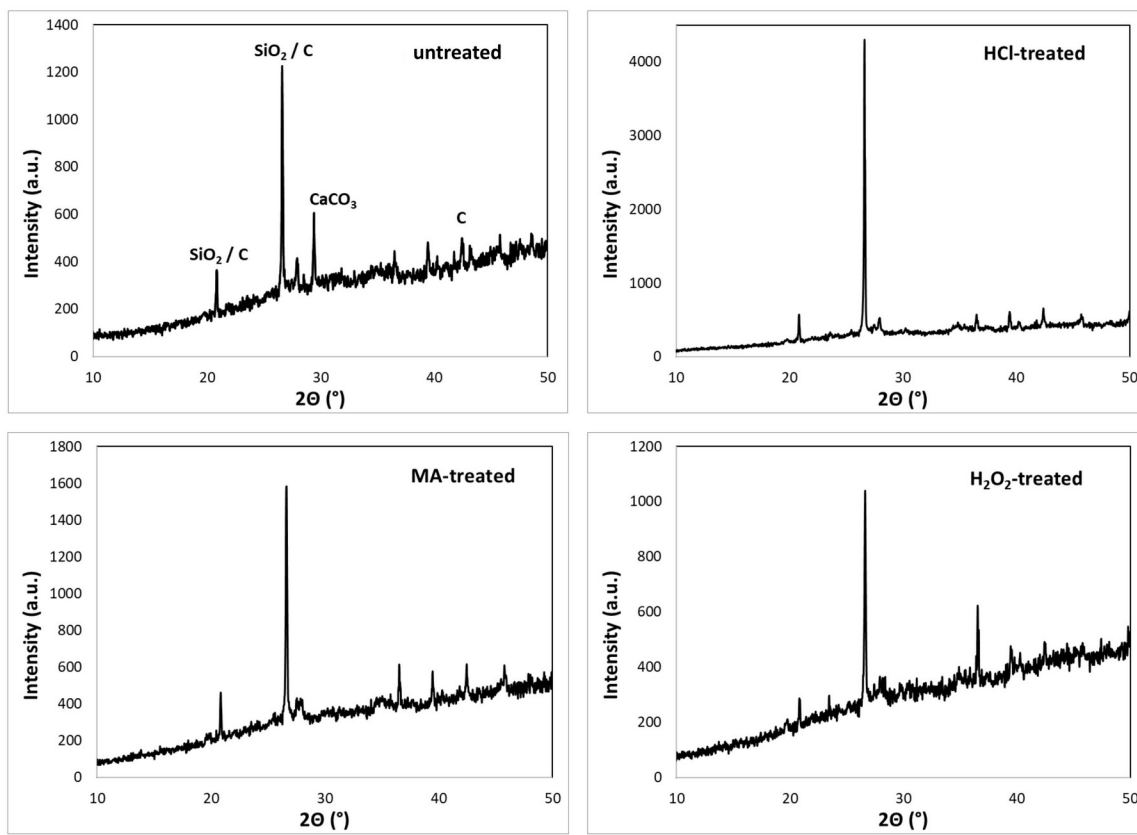


Fig. 3.

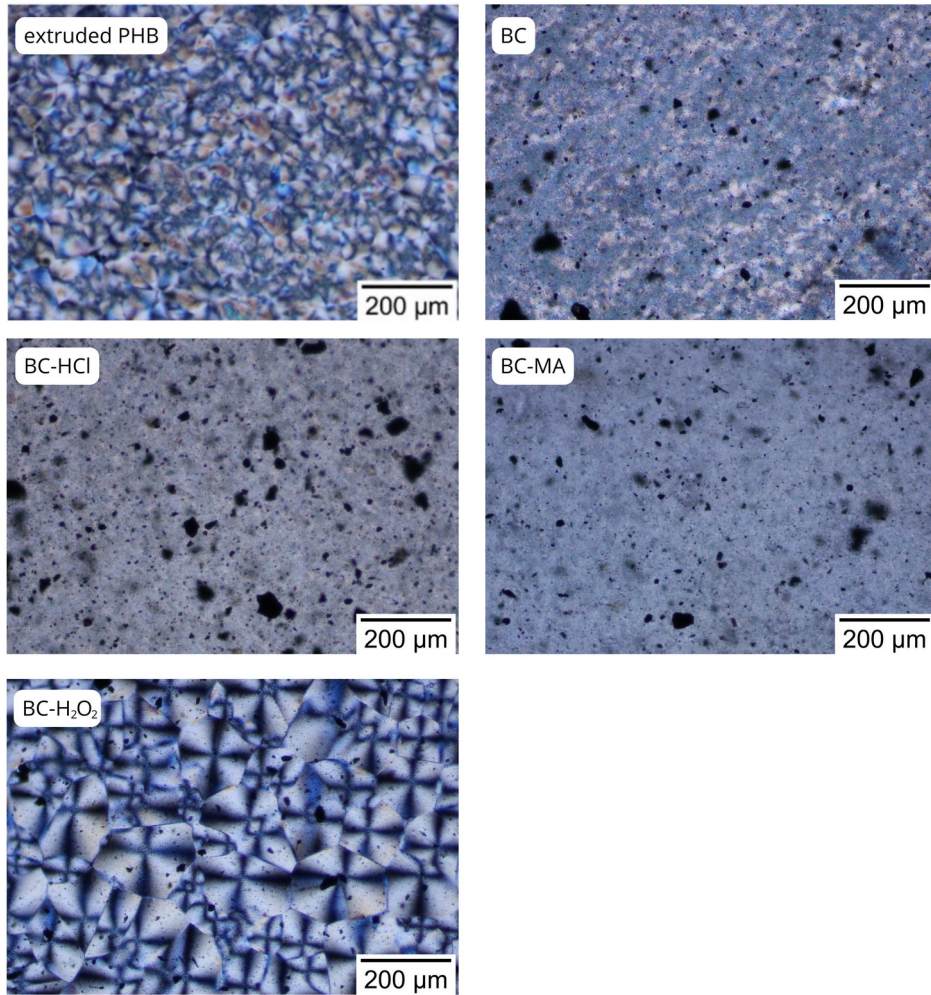


Fig. 4.

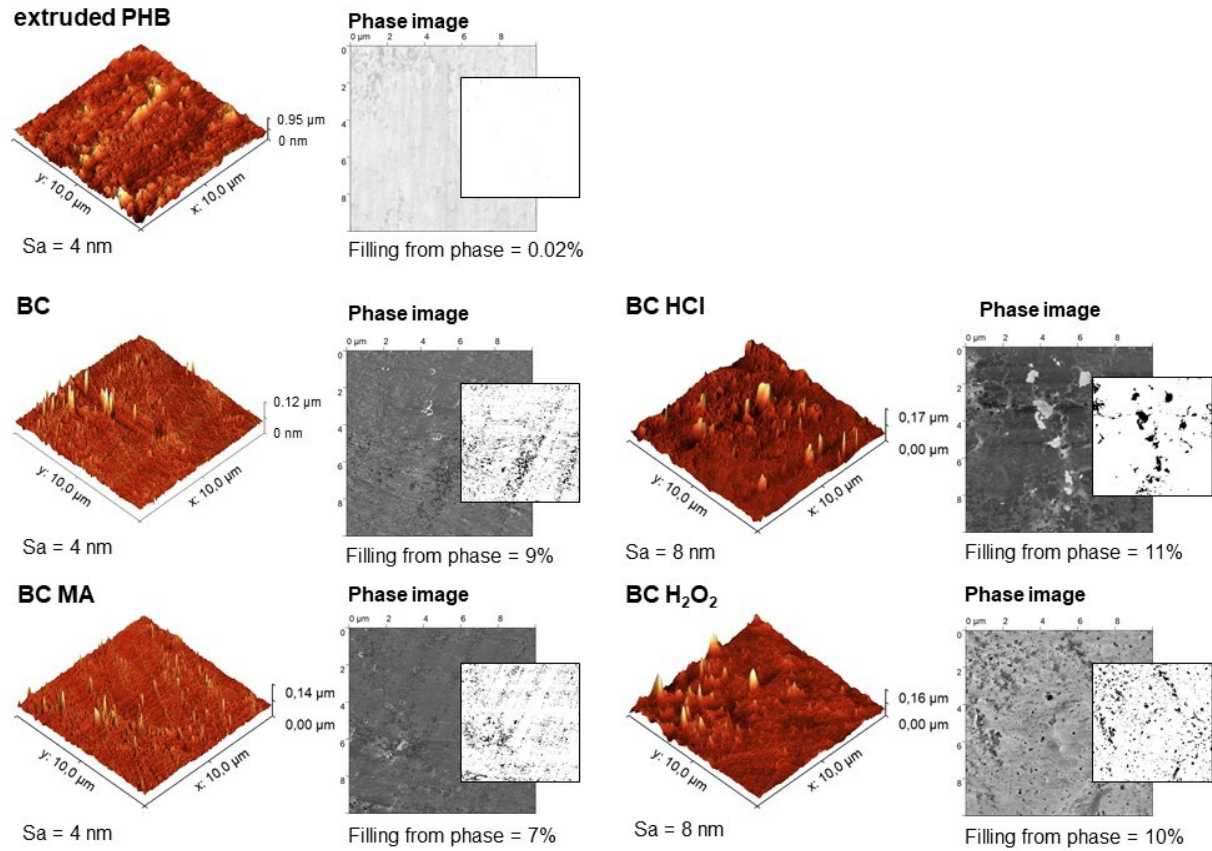


Fig. 5.

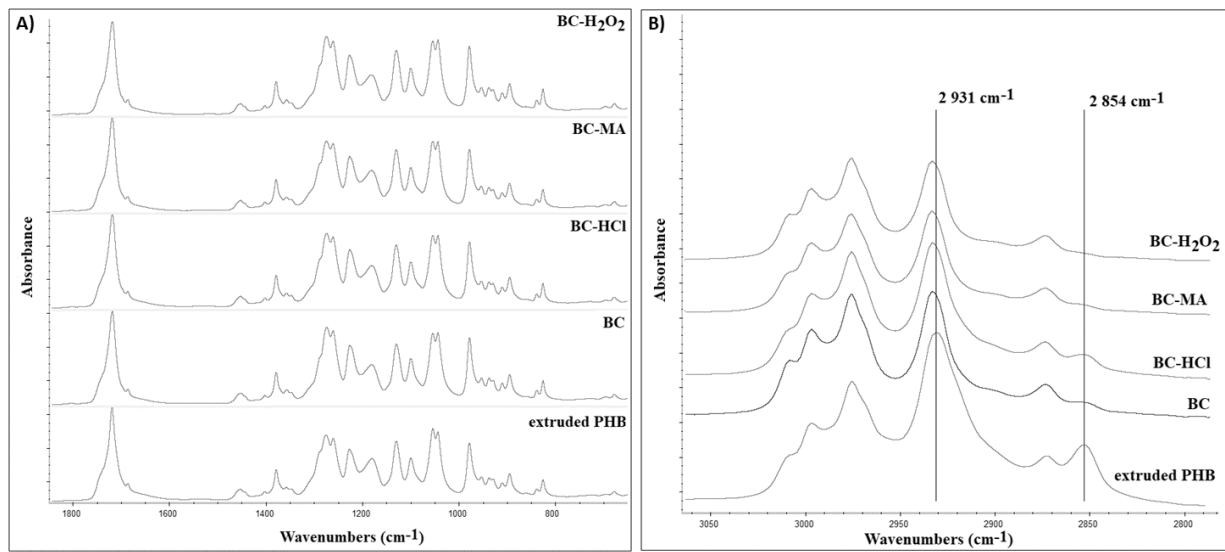


Fig. 6.

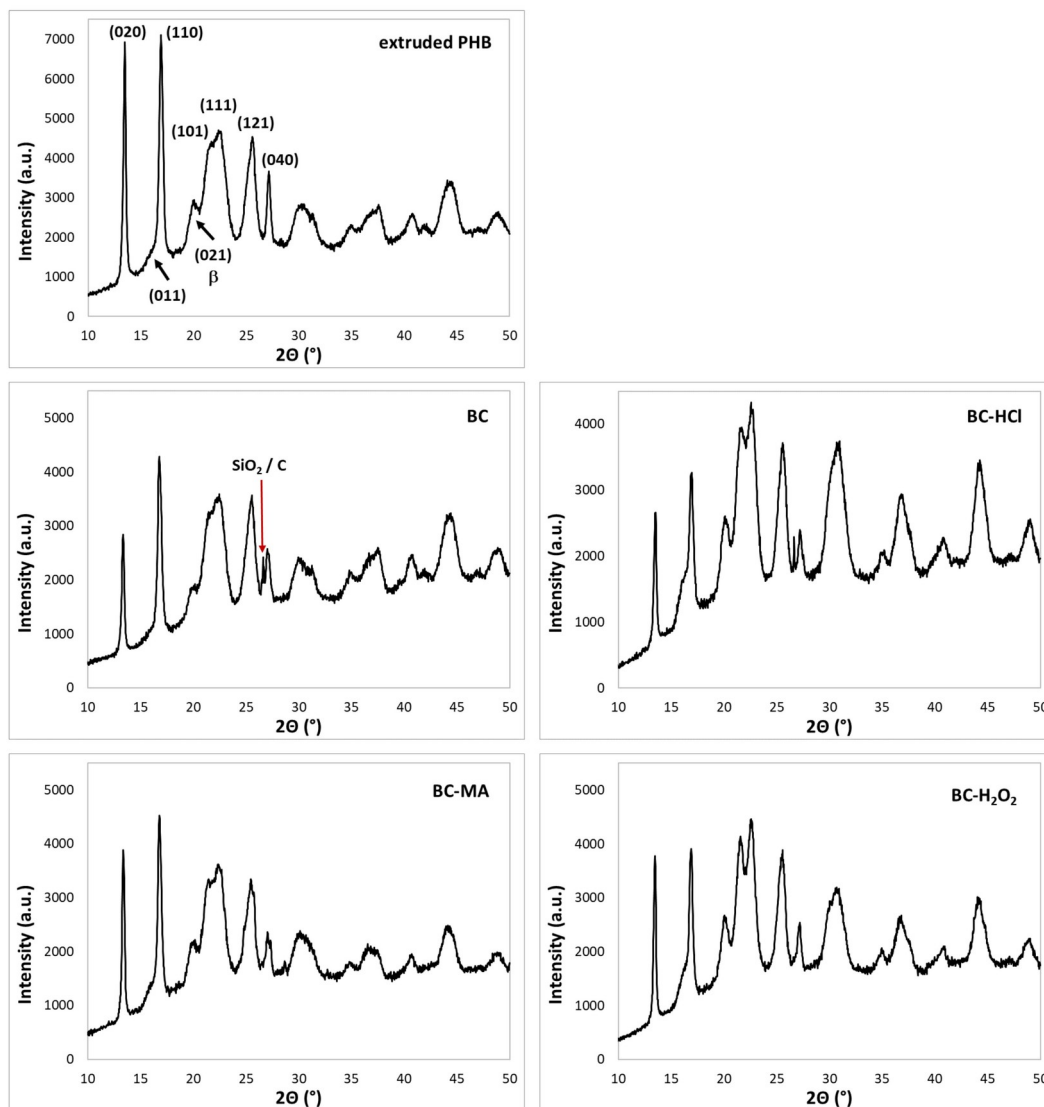


Fig. 7.

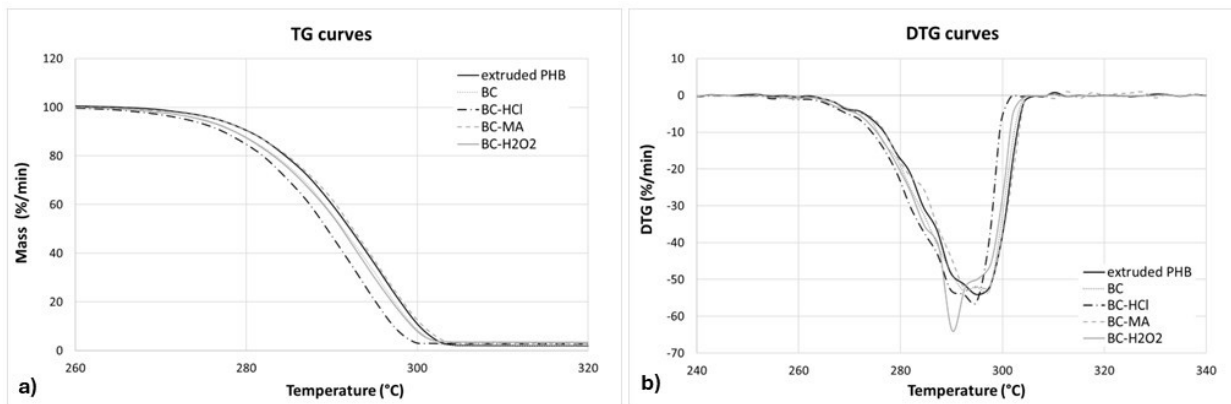


Fig. 8.

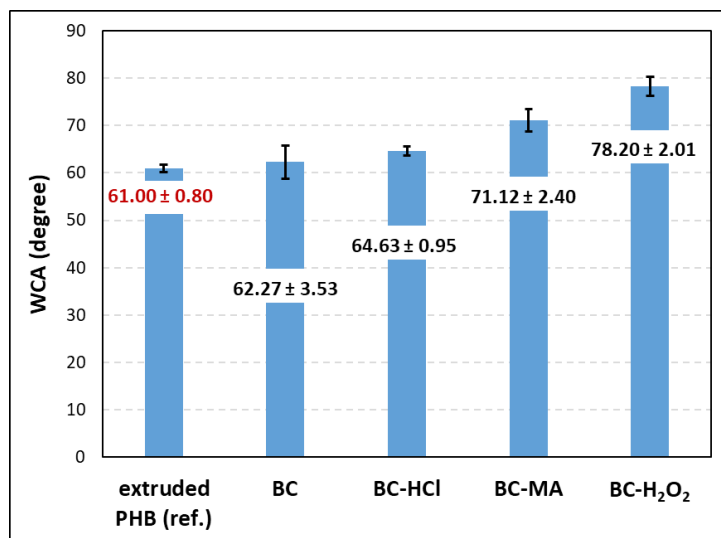


Fig. 9.

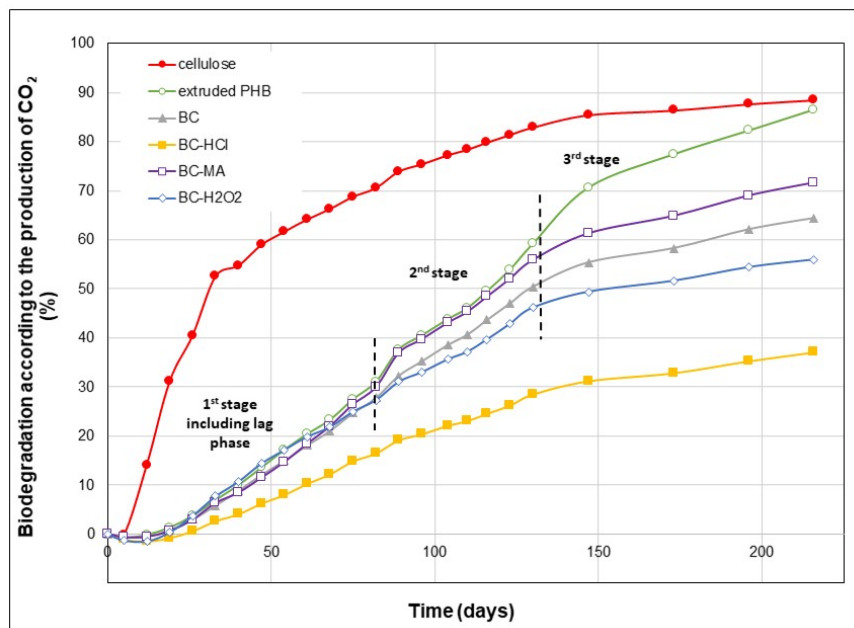


Fig. 10.

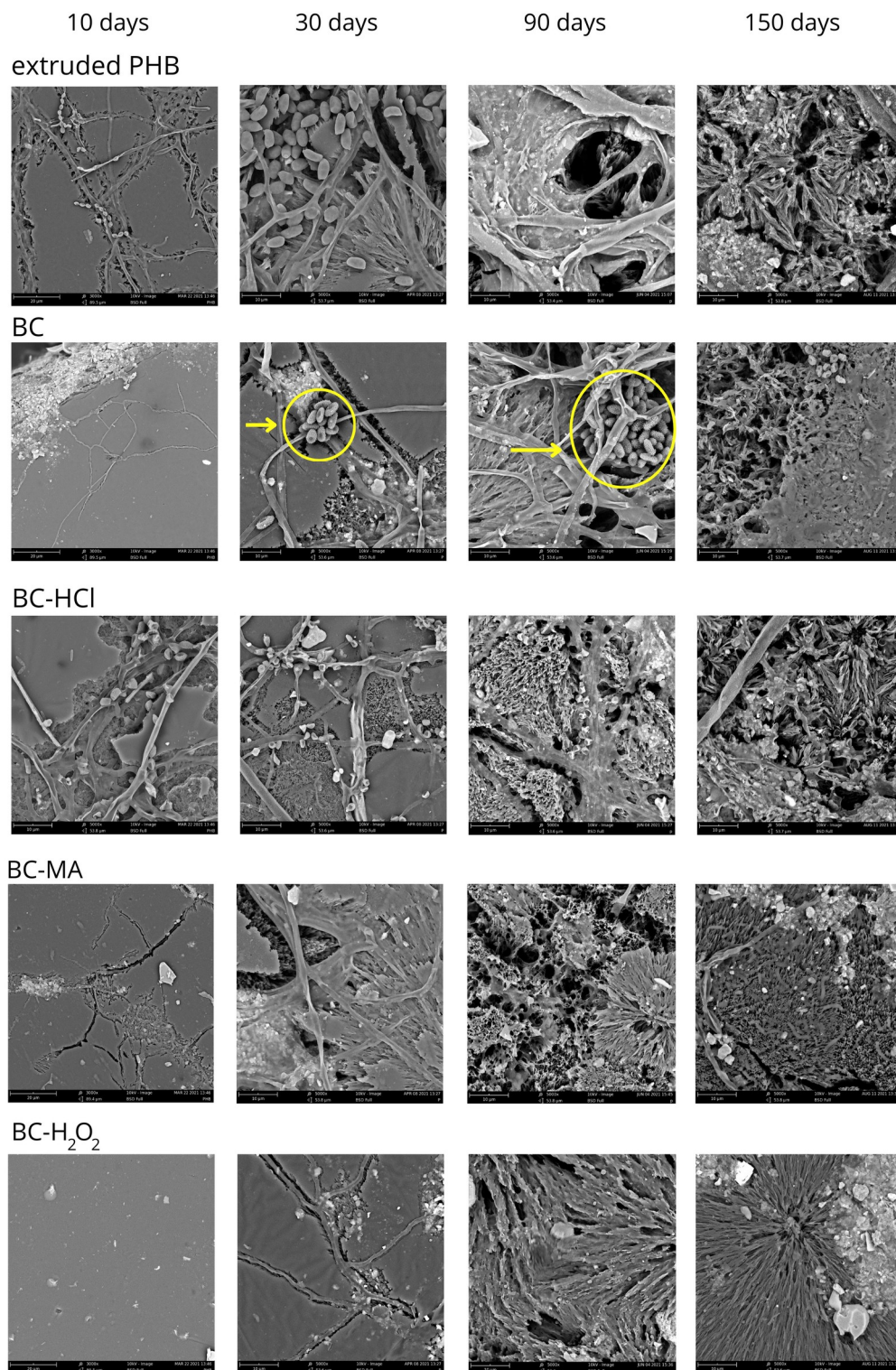


Fig. 11.

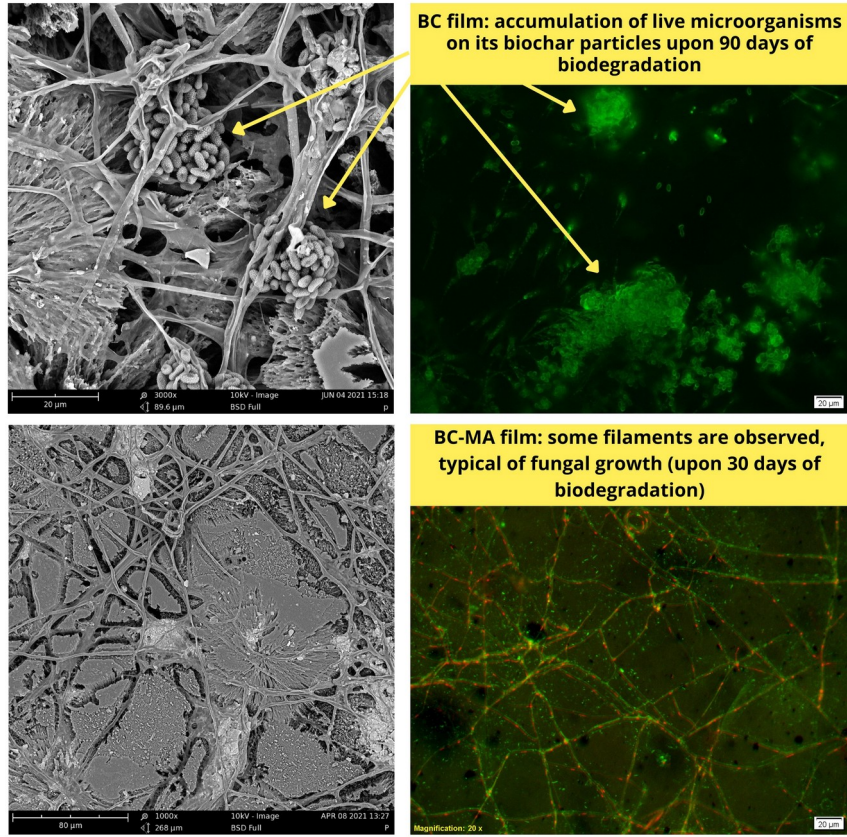


Fig. 12.

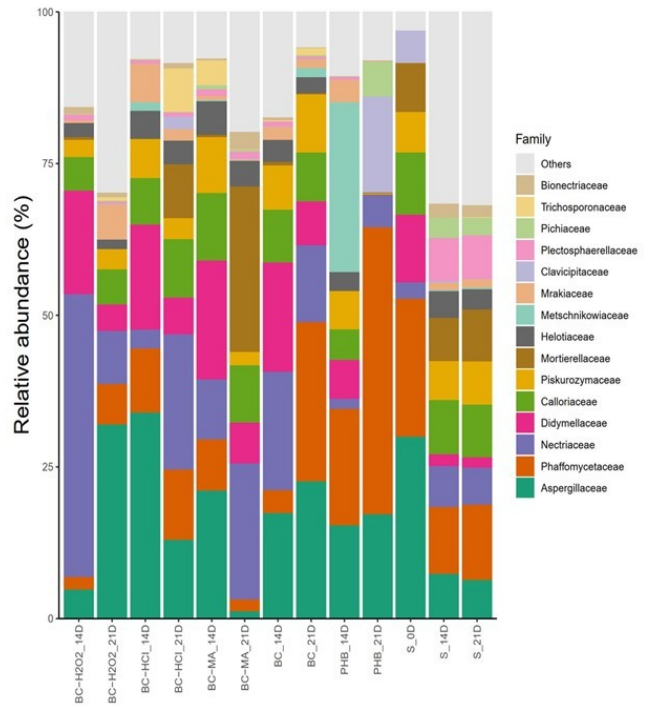
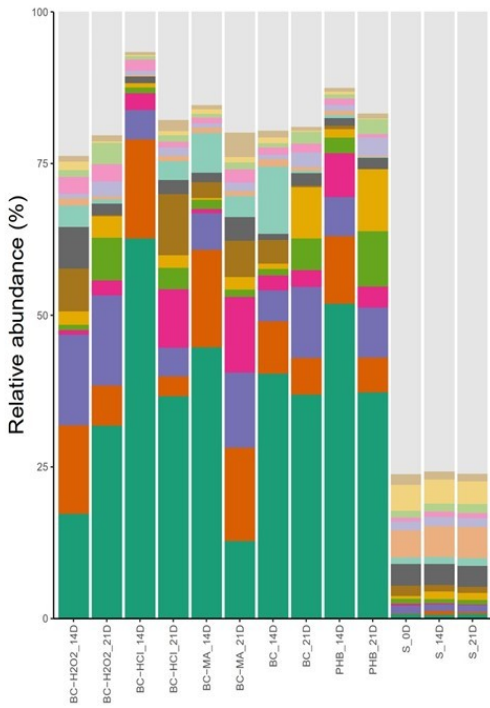


Fig. 13.

